A Mathematical Treatment of Integrated Ca Dynamics within the Ventricular Myocyte

Thomas R. Shannon,*[†] Fei Wang,[†] José Puglisi,[†] Christopher Weber,[†] and Donald M. Bers[†]

*Department of Molecular Biophysics and Physiology, Rush University, Chicago, Illinois; and [†]Department of Physiology, Loyola University-Chicago, Maywood, Illinois

ABSTRACT   We have developed a detailed mathematical model for Ca^{2+} handling and ionic currents in the rabbit ventricular myocyte. The objective was to develop a model that: 1), accurately reflects Ca-dependent Ca release; 2), uses realistic parameters, particularly those that concern Ca transport from the cytosol; 3), comes to steady state; 4), simulates basic excitation-contraction coupling phenomena; and 5), runs on a normal desktop computer. The model includes the following novel features: 1), the addition of a subsarcolemmal compartment to the other two commonly formulated cytosolic compartments (junctional and bulk) because ion channels in the membrane sense ion concentrations that differ from bulk; 2), the use of realistic cytosolic Ca buffering parameters; 3), a reversible sarcoplasmic reticulum (SR) Ca pump; 4), a scheme for Na-Ca exchange transport that is $[Na]_i$ dependent and allosterically regulated by $[Ca]_i$; and 5), a practical model of SR Ca release including both inactivation/adaptation and SR Ca load dependence. The data describe normal electrical activity and Ca handling characteristics of the cardiac myocyte and the SR Ca load dependence of these processes. The model includes a realistic balance of Ca removal mechanisms (e.g., SR Ca pump versus Na-Ca exchange), and the phenomena of rest decay and frequency-dependent inotropy. A particular emphasis is placed upon reproducing the nonlinear dependence of gain and fractional SR Ca release upon SR Ca load. We conclude that this model is more robust than many previously existing models and reproduces many experimental results using parameters based largely on experimental measurements in myocytes.

INTRODUCTION

[1]Cardiac myocyte excitation-contraction coupling (ECC) is an intricate process involving the interaction of a wide variety of systems, complexes, and proteins. Although it is possible to study each of these components in isolation, it becomes more and more difficult to obtain meaningful data when attempting to study the interaction of a number of these processes while they are working simultaneously. Mathematical modeling can be used to overcome these difficulties through the use of equations and parameters that accurately mimic laboratory experiments. These formulas can then be combined into a comprehensive whole to study their interactions. Such models are, and will always be, limited by the experimental data that are available and new data regarding cardiac excitation and contraction are constantly coming to light.

Where reliable experimental data exist, modeling data should be as consistent as possible with it. Models will never be as useful as laboratory data in terms of providing concrete information about physiological processes. The complexity of integrated physiological systems means a model will virtually never be perfect. Indeed, it is in this imperfection that we find perhaps a model's greatest usefulness. Where a model cannot be brought to describe experimental data, it identifies areas where our quantitative understanding is incomplete. The identification of these areas coupled with novel mathematical formulation allows the integrated model to be used as a powerful experimental tool to guide investigation and analytical thought.

There are many recent examples of mathematically modeled electrical and ionic homeostasis in the intact cardiac myocyte (McAllister et al., 1975; Beeler and Reuter, 1977; DiFrancesco and Noble, 1985; Priebe and Beuckelmann, 1998; Nordin, 1993; Pandit et al., 2003; Shiferaw et al., 2003; Bondarenko et al., 2004). Among the most valuable of these is the elegant model of Luo and Rudy (1994a,b), which does an outstanding job of modeling the individual currents that combine to produce a credible action potential (AP), and those of the Winslow group (Jafri et al., 1998; Winslow et al., 1999) that were a major step forward in modeling whole-cell Ca homeostasis. Each of these models has its distinct advantages and has proven useful in investigating a variety of different conditions and diseases such as heart failure (Winslow et al., 1999; Puglisi and Bers, 2001).

Since the introduction of many of these models in their original form, new information regarding the processes involved in ECC has become available. For instance, it is now well established that sarcoplasmic reticulum (SR) Ca content has a profound effect upon the process of Ca-induced Ca release (Spencer and Berlin, 1995, 1997; Janczewski et al., 1995; Bassani, J. W. M. et al., 1995; Donoso et al., 1995; Herrmann-Frank and Lehmann-Horn, 1996; Lukyanenko et al., 1996, 2001, 1999; Dettbarn and Palade, 1997; Satoh et al., 1997; Song et al., 1997; Eisner et al., 1998; Hüser et al., 1998; Kurebayashi and Ogawa, 1998; Shannon et al., 2000a, 2002b; Terentyev et al., 2002). This release results in an increase in Ca that appears to be higher just

under the sarcolemmal membrane (SL) than in the bulk cytosol and this higher [Ca] is detected by the Na-Ca exchanger and the Ca-dependent Cl channel, which are allosterically activated by it (Hilgemann et al., 1992; Matsuoka et al., 1995; Trafford et al., 1995; Weber et al., 2001, 2002).

With the above advances in mind, we have developed a new model of rabbit cardiac myocyte Ca and Na homeostasis. Our goals were fivefold: i), to track ion influx and efflux such that the model comes to steady state with a realistic balance of Ca fluxes; ii), to incorporate a form of Ca-induced Ca release (CICR); iii), to use realistic parameters that are consistent with laboratory observations; iv), to be able to simulate basic physiological phenomena when all of the components are combined; and v), to incorporate reasonable compromises to allow the model to be solved numerically on a desktop computer.

The model includes the following novel features: i), the addition of a subsarcolemmal compartment along with the junctional and bulk cytosolic compartments to allow proteins in the membrane to sense ion concentrations that differ from bulk; ii), the use of realistic cytosolic Ca buffering parameters; iii), a reversible SR Ca pump as suggested by the results of Shannon et al. (2000a); iv), a [Na]$_i$-dependent Na-Ca exchanger that is physiologically regulated by Ca as proposed by Hilgemann et al. (1992) (see also Weber et al., 2001); and v), a model of SR Ca release (Fabiato, 1985) including both inactivation/adaptation (Cheng et al., 1995; Stern et al., 1999) and SR Ca load dependence (Shannon et al., 2000b). The model data describe Ca handling characteristics of the cardiac myocyte and the SR Ca load dependence of these processes is accounted for. The model includes a realistic balance of cellular Ca removal mechanisms (Bassani et al., 1994; Puglisi et al., 1999) and the phenomena of rest decay and frequency-dependent inotropy. A particular emphasis is placed upon reproducing the nonlinear dependence of gain and fractional SR Ca release upon SR Ca load (Shannon et al., 2000a). We propose that this model is a robust representation that has useful characteristics not existent in previous models of excitation-contraction coupling (ECC).

MATERIALS AND METHODS

General approach

All programming was done on IBM PC desktop computers in the standard C programming language. Differential equations were solved using the CVODE package (http://www.netlib.org/ode/index.html). The described system of differential equations will typically generate a Ca transient (stimulation rate 1 Hz) in ~2 s on a Dell Precision 3500 workstation with Pentium 4 computer chip with 2.4-GHz processing speed and with 512 MB memory. The computation time was slowed by writing large numbers of parameters to the output text file. All simulations were done running Linux (Red Hat 9.0, Red Hat, Raleigh, NC).

The model is composed of a series of differential equations describing changes in [Ca], [Na], and membrane voltage over time. The AP is generally reconstructed from individual equations representing sarcolemmal membrane channels (Fig. 1) as in Luo and Rudy (1994a,b) with variations in and additions to individual equations and parameters as indicated below (see also Puglisi and Bers, 2001). Markovian channel models were generally avoided unless they were determined to be necessary. Such models often add additional differential equations to the model that must be solved, thus slowing the computation time.

Cellular structure

The 33 pL cell is separated into four lumped compartments (Fig. 1 A): i), the SR (3.5% of the cell volume; Page et al., 1971); ii), the junctional cleft (0.077% assuming 11% of the cell membrane is junctional and that the cleft is 15-nm deep; Page and Surdyk-Droske, 1979; Soeller and Cannell, 1997); iii), the subsarcolemmal space (2% assuming 89% of the membrane is nonjunctional SL and by making the space 45-nm deep); and iv), the bulk cytosolic space (65% with the remainder of the volume accounted for by mitochondria; Page et al., 1971). The accessible cleft volume is reduced by an additional third to 0.051% due to the occupation of this space by protein (Soeller and Cannell, 1997). Cellular dimensions and environmental parameters are located in Table 2.

The junction was considered to be a disk of radius 160 nm and 15 nm in depth. Diffusion is restricted in this space due to its narrow boundaries (i.e., by the SR membrane and the SL membrane) and by the large proteins within the cleft (e.g., the RyR). The number of these when spaced evenly 1.2 μm apart from center to center over the entire cell membrane area of 15,000 μm^2 (4.58 pF/pL, 1 μF/cm^2; Satoh et al., 1996) is 20,000 (Fig. 1 B).

This spacing of junctions also gives a distance of diffusion to the middle of the SL compartment of 500 nm. This is a narrow space just under the SL membrane that is diffusionally restricted on the cytosolic side by such structures as the mitochondria and the myofilament array. Similarly, an average distance of diffusion of 0.45 μm from the SL to the middle of the half sarcomere (i.e., the cytosolic compartment) was also calculated assuming a sarcomere length of 1.8 μm. These diffusional distances dictate the transfer functions for the fluxes between each compartment. This adjusts the lumped nature of the compartments to an appropriate physical geometry.

Na buffers were located only in the junction and SL compartment and were modeled as rapidly binding molecules with the standard Hill equation (Eq. 14, Table 3; parameters were taken from Bers et al., 1986).

Ca buffers were distributed in each compartment as appropriate (Table 7). SR Ca buffers (primarily calsequestrin) were modeled as rapidly binding molecules. Parameters are from Shannon and Bers (1997) and Shannon et al. (2000). Cytosolic Ca binding molecules were modeled in a time-dependent manner (Eq. 76) Parameters are generally as in Shannon et al. (2000). Dyes such as indo-1 and fluo-3 were not included in the simulations. However, when these dyes were added at a concentration of 25 μM, they reduced the peak Ca transient by ≈20% and slowed the rate of steady-state Ca transient decline with stimulation at 0.5 Hz by ≈15% (data not shown).

Sarcolemmal ion transport

Changes in cell Na and Ca were modeled for rabbit at 37°C. Where appropriate, the temperature-dependent parameters were changed as described in the Appendix. The rate of change in total ion concentration ($d[Na]_T/dt$, $d[Ca]_T/dt$) was calculated from the total ion flux in ($d[Na]_{in}/dt$, $d[Ca]_{in}/dt$) and the total ion flux out ($d[Na]_{out}/dt$, $d[Ca]_{out}/dt$) and integrated:

$$\frac{d[Na]_T}{dt} = \frac{d[Na]_{in}}{dt} - \frac{d[Na]_{out}}{dt} \tag{1}$$

$$\frac{d[Na]_{in}}{dt} = I_{Na} + I_{NCX\text{-}Na} + I_{NaBk} \tag{2}$$

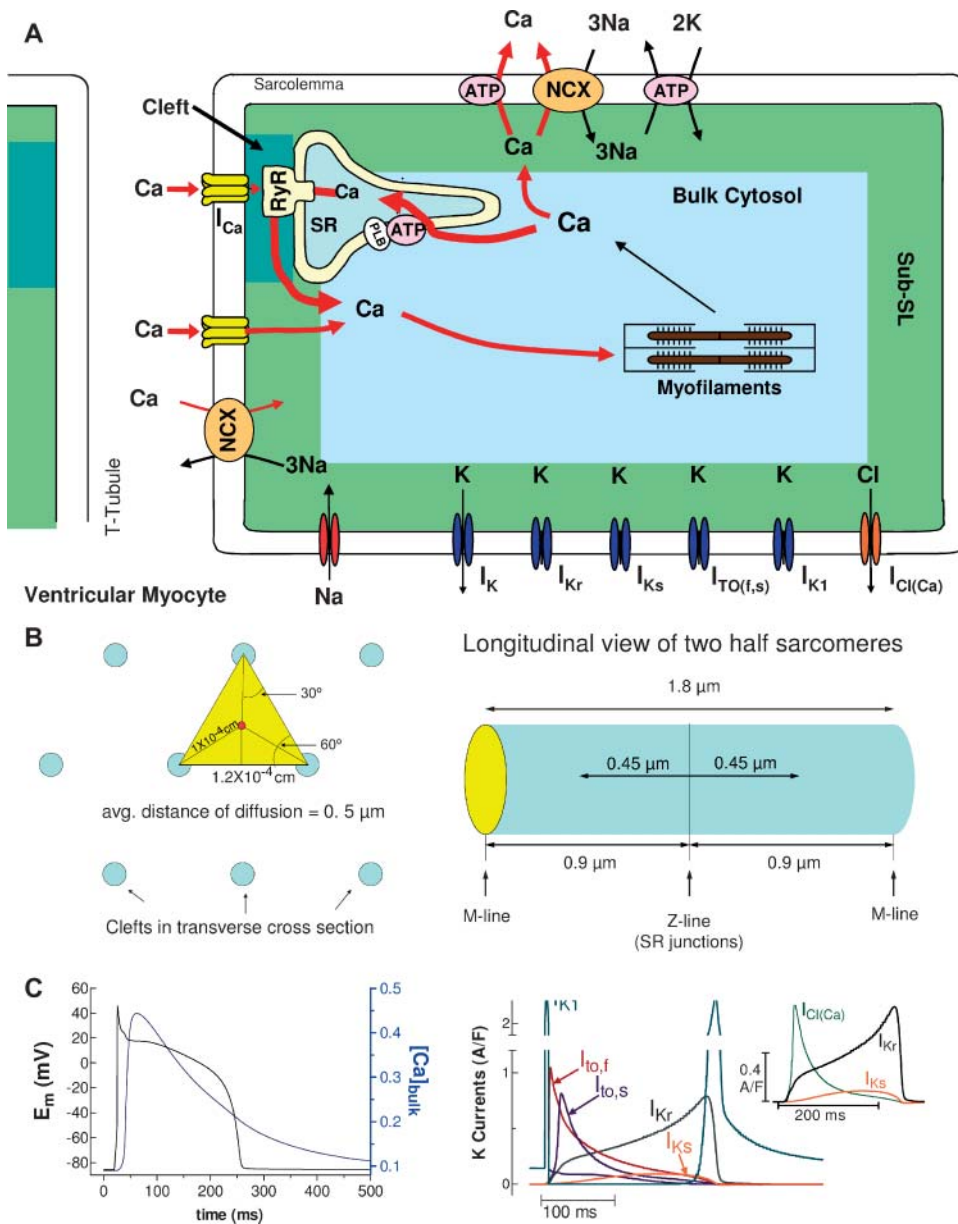$$\frac{d[Na]_{out}}{dt} = I_{NaK} \tag{3}$$

FIGURE 1 (*A*) Diagram of the cell with Ca- and Na-dependent components of the model. (*B*) Diagrams of the arrangement of junctions over the area of the cell membrane (*left*) and of the cytosolic space of the sarcomere. Diffusion distances were calculated based upon this arrangement from the center of each compartment assuming that each junction contributed an equal amount of Ca to each space. (*C*) (*Left*) An action potential and the accompanying bulk cytosolic Ca transient. (*Right*) Relevant K and Cl currents. (see Materials and Methods above; Puglisi and Bers, 2001)

$$\frac{d[Ca]_{\mathrm{T}}}{dt} = \frac{d[Ca]_{\mathrm{in}}}{dt} - \frac{d[Ca]_{\mathrm{out}}}{dt} \qquad (4)$$

$$\frac{d[Ca]_{\mathrm{in}}}{dt} = I_{\mathrm{Ca}} + I_{\mathrm{CaBk}} \qquad (5)$$

$$\frac{d[Ca]_{\mathrm{out}}}{dt} = I_{\mathrm{NCX}} + I_{\mathrm{SLCaP}}, \qquad (6)$$

where I_{Na} is fast Na current (Eq. 37), I_{NaBk} is Na leak (Eq. 38), I_{NaK} is Na-K pump current (Eq. 41), I_{Ca} is L-type Ca current (Eq. 93), I_{CaBk} is SL Ca leak (Eq. 94), I_{NCX} is Na-Ca exchange current (Eq 96), and I_{SLCaP} is SL Ca pump transport (Eq. 97).

I_{NaBk} and I_{NaK} were formulated as previously (Luo and Rudy, 1994a,b; Puglisi and Bers, 2001) and were adjusted to give resting flux values similar to those measured experimentally by Despa et al. (2002a,b).

Ca currents

Ca current was formulated as previously described (Luo and Rudy, 1994a,b; Puglisi and Bers, 2001) with modifications. The formulations are based upon the Goldman-Hodgkin-Katz equation. The permeabilities of the L-type Ca channels for Na and K were decreased, consistent with the selectivity of the channel for these ions in the presence of Ca in the perfusate (Hess et al., 1986; Tsien et al., 1987). Currents were scaled to approximate those of Puglisi et al. (1999). Ca-dependent inactivation was modified to be calmodulin dependent (Eq. 77; Peterson et al., 1999; Qin et al., 1999). Kinetics of binding were set with a K_{d} of 7 μM to give typical experimental values for the fast and slow time constants of decline in I_{Ca} due to inactivation during a normal Ca release

(3 and 28 ms, respectively), when a depolarization from -40 to 0 mV was simulated (Eq. 78). Ninety percent of the channels are located in the junctional cleft membrane (Scriven et al., 2000). T-type Ca current was not included in the model because this current, although present in some cardiomyocytes (Bean, 1989; Nuss and Houser, 1993), is undetectable in normal rabbit ventricular myocytes (Yuan et al., 1996).

The SL Ca leak flux was adjusted to match that calculated from Negretti et al. (1993). The SL Ca pump was formulated using the standard Hill equation and approximates cellular estimates of Bassani et al. (1994).

The Na-Ca exchanger was formulated essentially as described in Weber et al. (2001). The scheme is a general improvement over other models in that it is $[Na]_i$ dependent and allosterically regulated by Ca. As with all of the channels and transporters with the exception of the L-type Ca channel, Na-Ca exchange molecules were evenly distributed throughout the cell membrane, 89% in the SL compartment and 11% in the junctional membrane.

Sarcoplasmic reticulum Ca transport

Ca transport out of the SR into the cytosol was calculated:

$$J_{SR} = J_{rel} - J_{pump} \qquad (7)$$

where J_{rel} is the SR Ca release flux (Eq. 106) and J_{pump} is the SR Ca pump flux (Eq. 98). The SR Ca pump is a reversible enzyme formulated as in Shannon et al. (2000a). It is important to note that the net SR Ca pump rate never reverses. The enzyme merely slows as product ($[Ca]_{SR}$) builds up. All of the SR Ca pump molecules were localized to the cytosolic compartment (Fig. 1).

The cytosolic Ca dependence of the SR Ca release channel (RyR) was modeled in a steady-state manner as in Stern et al. (1999) (see Fig. 4 A, based upon Fabiato, 1985 and Cheng et al., 1995). The model has four states: resting or closed (R), open (O), inactivated (I), and resting inactivated (RI). Models of this type are typically used by investigators working on single-channel RyR gating (Scheifer et al., 1995; Zahradnikova and Zahradnik, 1996; Keizer and Levine, 1996; Villalba-Galea et al., 1998). Additional states are often added to such models but this one with our modifications (e.g., lumenal $[Ca]_{SR}$ dependence) works well.

During a typical Ca release cycle, the RyR exists predominantly in the closed state. Upon depolarization and sudden Ca influx into the cleft, Ca binds to the cytosolic activation site on the RyR resulting in a transition to the open state. Ca also binds to the slower cytosolic inactivation sites resulting in the transition from the open state to the inactivated state. As Ca declines, there is a transition to the resting inactivated state and finally back to the closed state.

SR Ca load dependence was added as a lumenal Ca binding site that affects the state of the RyR. Ca binding to this site affects both the inactivation and activation cytosolic Ca-dependent rate binding constants (Eqs. 99–101). Neither rate constant was allowed to exceed diffusional limitations for Ca binding. When Ca is bound on the lumenal side and this site is occupied, the affinity of the cytosolic activation site increases whereas the affinity of the inactivation site decreases. Thus, there is a greater tendency for the RyR to undergo transition to the open state. On the other hand, when less Ca is bound to the lumenal site, there is a greater tendency for the RyR to exist in the inactivated state.

All of the SR Ca release takes place in the junctional compartment. A passive leak from the SR into the junctional compartment was also added to give a total diastolic leak (passive and diastolic RyR leak) of ≈ 4 $\mu M/s$ (Shannon et al., 2001).

Other currents

Most K currents were formulated as by Luo and Rudy (1994a,b) as modified by Puglisi and Bers (2001) and Bassani et al. (2004). Two notable exceptions are in the I_{Ks} current and the Ca-dependent Cl current (I_{Cl}). I_{Ks}

was modeled to resemble the data of Tohse (1990). In accordance with this article, currents were made Ca dependent and were scaled as appropriate for the rabbit. Cl currents were added to the model and scaled to approximate those of Zygmunt and Gibbons (1991) and Puglisi et al. (1996) using a K_d for Ca of 100 μM (Collier et al., 1996)

RESULTS

During excitation-contraction coupling, Ca enters through Ca channels in response to an action potential (Figs. 1 and 2). The AP in our model is formulated by combining equations that describe the characteristics of the voltage-dependent ion channels in isolation into a coherent model. The equations used for the Na and K currents are based upon those of Luo and Rudy (1994a,b) with some modifications (Jafri et al., 1998; Puglisi and Bers, 2001; Bassani et al., 2004). Combined, the currents produce a relatively normal AP waveform with a duration of 235 ms.

The I_{Ks} current has also been modified to be Ca dependent (Eq. 57) (Tohse, 1990) and a Ca-dependent Cl current was added (Zygmunt and Gibbons, 1991). Selective blockade of I_{Kr} and or I_{Ks} in the model produces the expected action potential duration changes as measured in rabbit ventricular myocytes (data not shown; Salata et al., 1996). The Ca dependence of these currents highlights a major change in the model that differentiates it from formulations previously proposed. All of the Ca-dependent SL membrane processes are now dependent upon the [Ca] within a separate physiological compartment. The existence of this compartment is inferred by data indicating that the [Ca] just underneath the SL membrane peaks at a higher level than is present in the bulk cytosol (Trafford et al., 1995; Weber et al., 2001). By formulating the behavior of these proteins based upon the [Ca] within the SL compartment, we have been able to profile their contribution to the overall physiology of the cell in a more realistic way consistent with their biochemical characteristics.

In our model 90% of the Ca channels are located in the junction based upon the data of Scriven et al. (2000, 2002) who found that the vast majority of the channels colocalize with the RyR. AP-dependent Ca currents tend to be of variable shape (Fig. 2 B; Linz and Meyer, 1998; Puglisi et al., 1999; Linz and Meyer, 2000). This variability is species dependent and may be due to changes in the shape of the AP, to the effects of temperature, and to the effects of released Ca upon the current. Ca-dependent inactivation of the L-type Ca channel is accounted for within the model and changes in the released Ca also cause the expected changes in the shape of the Ca current (Fig. 5 B; see below). The shape of the current in the model with a normal release during 1-Hz pacing is typical (Fig. 2 B; see also Fig. 5 B).

The rise in free junctional cleft [Ca] ($[Ca]_{jct}$) resulting from L-type Ca current initiates CICR. Ca in the cleft peaks very early at a high value before diffusing through the SL compartment to the cytosol. The cytosolic Ca transient
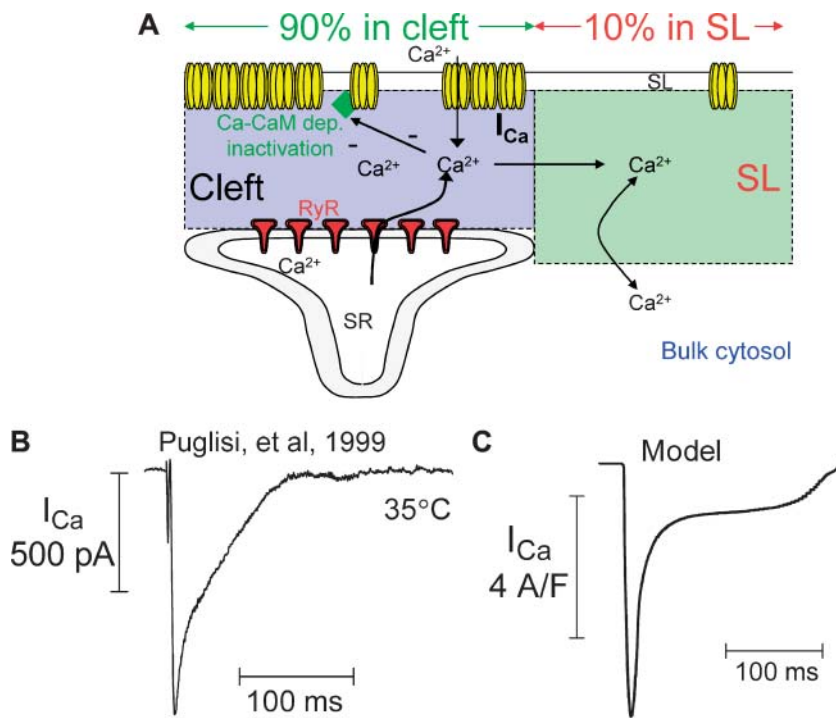
FIGURE 2 (*A*) Diagram of the way in which the L-type Ca channel operates. The model includes Ca-dependent inactivation that is Ca-calmodulin (CaM) dependent. Most of the channels (90%) are in the cleft space (Scriven et al., 2002). (*B*) L-type Ca current generated during the AP (*right*). The currents of Puglisi et al. (1999) are shown for comparison (*left*).

matches that normally observed in cardiac myocytes (Fig. 3 *B*). The time constant for $[Ca]_i$ transient decline (190 ms) is similar to experimental data at 35–37°C (Puglisi et al., 1996). The character of the submembrane SL Ca transient is similar to that estimated by Weber et al. (2002) (Fig. 3 *C*), peaking at a value well above the peak of the cytosolic Ca transient, and falling as Ca diffusion into the bulk cytosol takes place, eventually converging with the bulk $[Ca]_i$ transient.

The RyR was modeled essentially as in Stern et al. (1999) with the significant addition of a dependence of RyR gating upon $[Ca]_{SR}$ (Fig. 4 *A*). The SR Ca release flux rises rapidly

to a peak (Fig. 4 *B*) that matches that of Sipido and Wier (1991) and Shannon et al. (2000b). This flux falls rapidly as Ca diffuses from the junctional cleft and as the channel transitions from the open state (Figs. 4, *C* and *D*) into the inactivated state. Note also that because the binding to both the cytosolic activation and inactivation is dependent upon the SR Ca concentration, the fall in this concentration also plays a role in facilitating this transition. Finally the RyR shifts into the resting inactivated state and eventually back to the resting state. Note well the rate of recovery from inactivation back to the closed (R) state. The rate of this
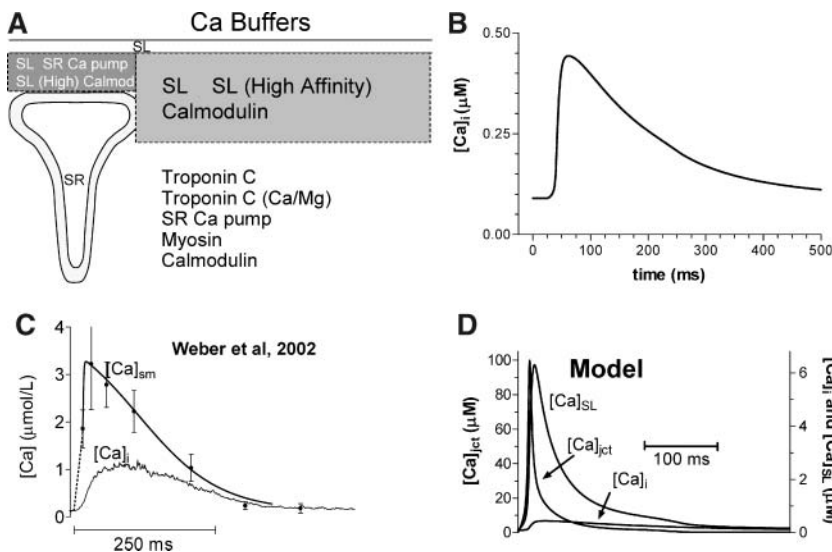

FIGURE 3 (*A*) Ca buffers in each compartment. (*B*) Bulk cytosolic Ca transient. (*C*) Ca transients in each of the three non-SR compartments. Data are compared to that of Weber et al. (2002).
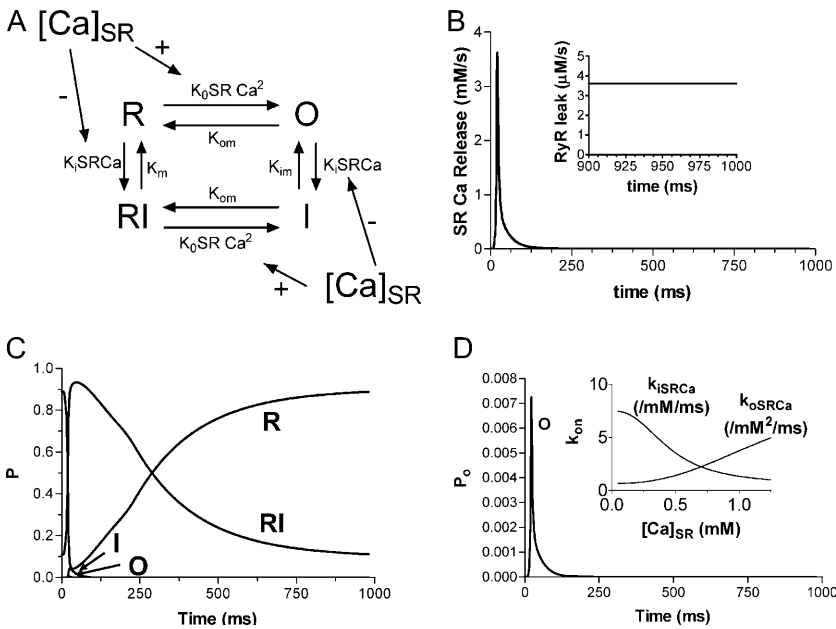
FIGURE 4 (A) Markovian state model of the ryanodine receptor. The model was developed from that of Stern et al. (1999) with the addition of SR Ca load dependence to the binding of Ca to the activation and inactivation cytosolic sites. (B) SR Ca release flux with RyR-dependent SR Ca leak (inset). Total leak is equal to this diastolic release plus the passive leak flux (4 μM/s). (C) Profile of the four channel states over the course of an AP. (D) Time-dependent profile of the channel open state with changes in the k_{on} for Ca binding with $[Ca]_{SR}$ (inset).

transition is consistent with estimates for recovery of the RyR based upon availability for Ca release in intact isolated myocytes ($\tau = 650$ ms; Bers, 2001; Cheng et al., 1996). This recovery is related in part to the reuptake of Ca back into the SR during diastole. The resulting higher $[Ca]_{SR}$ favors the closed state of the channel.

The Ca dependence of release was tested by simulating a standard experimental assay for ECC. The digital cell was stimulated to steady state with 200-ms square pulses to 0 mV and a test pulse was applied to varying voltages from -60 to

$+40$ mV. The release of Ca from the SR was graded and dependent upon the L-type Ca current (Fig. 5 A).

Importantly, released Ca also has a major effect upon the L-type Ca current. As would be expected in an isolated myocyte, this current exhibits Ca-dependent inactivation in the model. This inactivation is known to be dependent upon Ca binding to calmodulin (Peterson et al., 1999; Qin et al., 1999). Fig. 5 B graphically shows the effect of this Ca binding in the model. Ca current with normal release into the cleft inactivates rapidly as would be expected. On the other
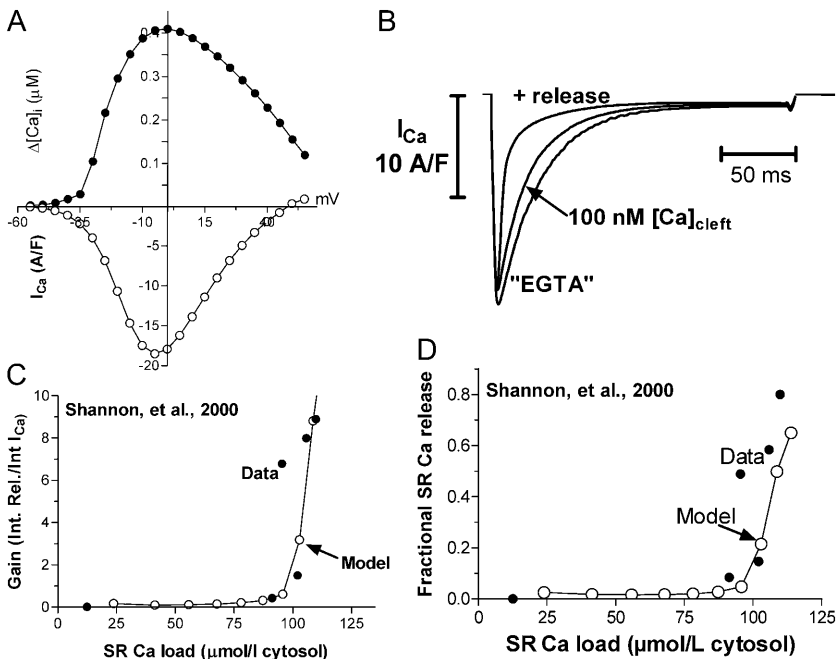

FIGURE 5 (A) CICR in response to graded L-type Ca current. The change in the bulk Ca during the transients and the integrated SR Ca release (top) correspond to the peak L-type Ca currents (bottom) at each voltage. (B) L-type Ca current in response to a 200-ms square pulse to 0 mV from a holding potential of -80 mV. Currents show normal Ca-dependent inactivation of current in the presence of release and with Ca buffered to 100 nM when compared to "EGTA" currents with no Ca-dependent inactivation. I_{Ca} and integrated SR Ca release are normalized to their peaks (0.410 μM and 57.4 μmol/l cytosol, respectively). (C) $[Ca]_{SRT}$ dependence of the gain (left) and fractional release (right). The data of Shannon et al. (2000a) are shown for comparison ($\bullet$).

hand, Ca current with no release and Ca current with $[Ca]_{jct}$ clamped at 100 nM inactivates slower due to reduced Ca binding to the channel/calmodulin complex.

Similarly, Ca release was tested as a function of $[Ca]_{SRT}$. Experiments by Shannon et al. (2000a) were simulated. After depletion of SR Ca, the cell was depolarized to 0 mV for 200 ms per pulse in the absence of Na inside and outside of the cell. The absence of Na prevented Na-Ca exchange from operating, which causes the retention of nearly all Ca brought in by the L-type Ca current within the cell. Most of the Ca is retained within the SR resulting in a larger release with each successive depolarization. The model simulates the actual data indicating normal $[Ca]_{SRT}$-dependent release (Fig. 5, C and D).

The overall physiology of the release from the SR is also in agreement with laboratory data. J. Bassani et al. (1993b, 1995) found that the fractional release from the SR during the $[Ca]_i$ transient is 50%, which agrees well with the model as do the $[Ca]_{SR}$ transients of Shannon et al. (2003a) (Fig. 6, A and B). Fig. 6 A shows the effect of removing the lumenal regulation from the SR Ca release process. The first beat upon removal of the regulation has a larger fractional release with a longer time to peak.

Ca diffuses from the junctional cleft to the SL compartment and is transported by two sarcolemmal transporters. The Na-Ca exchanger and the SL Ca pump transport Ca from the junctional cleft and the SL compartment to the extracellular compartment. At steady state, the integrated fluxes through these transporters is equal to the amount of Ca that enters primarily through the L-type Ca channels (with a small amount of Ca entry via Na-Ca exchange; see below).

The formulation of the Na-Ca exchanger is based upon that used in Weber et al. (2001) and the modeled current during the AP is similar to the actual data (Fig. 7). In contrast to previous formulations used in whole-cell simulations (Luo and Rudy, 1994a; Jafri et al., 1998), the equation accounts for the $[Ca]_{SL}$-dependent activation of Na-Ca exchange that takes place during the Ca transient. Note once again that this activation depends upon $[Ca]_{SL}$, i.e., the [Ca] just under the SL membrane that is actually sensed by the exchange protein. The equation also accounts for the effects of intracellular [Na] at the transport site, specifically Na just underneath the SL membrane in the SL compartment, another important addition.

This Na-Ca exchanger indirectly competes with the SR Ca pump for Ca. The SR Ca pump formulation used in this model is that proposed by Shannon et al. (2000a) and the Ca pump flux (Fig. 6 B) is very similar to the flux calculated from the data there. The pump is modeled as a reversible enzyme, mediating both ''forward'' and ''reverse'' unidirectional fluxes. The net flux into the SR is the difference between the two flues. In other words, the transporter can be thought of as a reversible enzyme with $[Ca]_i$ as the substrate and $[Ca]_{SR}$ as the product. The net transport rate from the cytosol to the SR rises during the release as cytosolic [Ca] (the substrate) rises and SR [Ca] (the product) falls. This causes a tendency for the pump to operate in the forward mode, transporting more Ca into the SR. As $[Ca]_{SR}$ rises and $[Ca]_i$ falls the rate of uptake falls as the unidirectional reversal flux rises and the forward flux decreases. The amount transported in one beat at steady state is equal to the amount released.

The transport competition among Na-Ca exchange, the SR Ca pump, and the SL Ca pump takes place in a characteristic, species-dependent way (Bassani et al., 1994). The balance of integrated fluxes in rabbit cardiac myocytes is depicted in

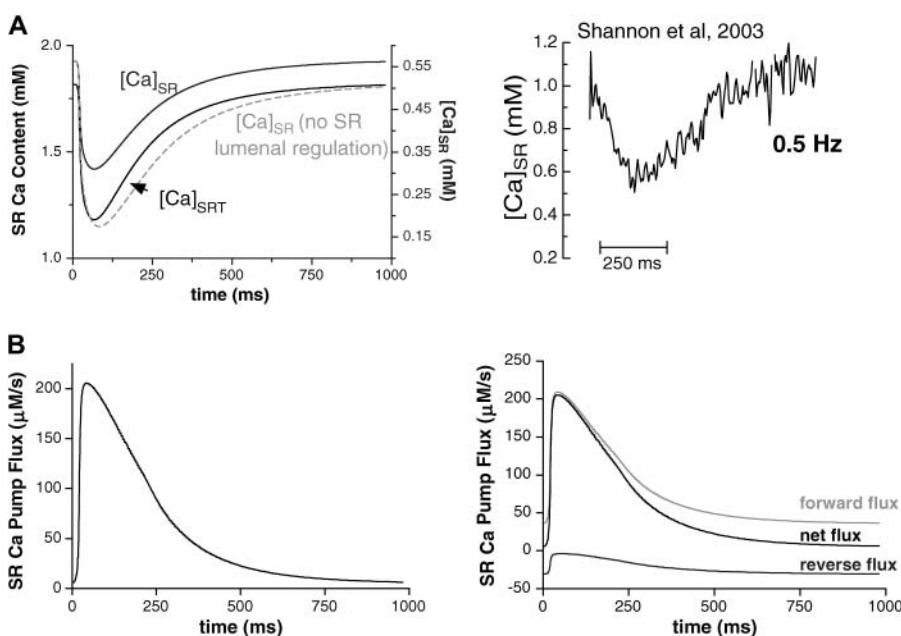FIGURE 6 (A) Changes in $[Ca]_{SRT}$ and $[Ca]_{SR}$ over the time course of the Ca transient. The fractional release (30%) agrees well with the value measured by J. Bassani et al. (1993b, 1995). The $[Ca]_{SR}$ transient agrees well with the data of Shannon et al. (2003) (B) Net SR Ca pump flux (*left*) into the SR, which is the difference between the forward and reverse unidirectional fluxes (*right*) (Shannon et al., 2003a).
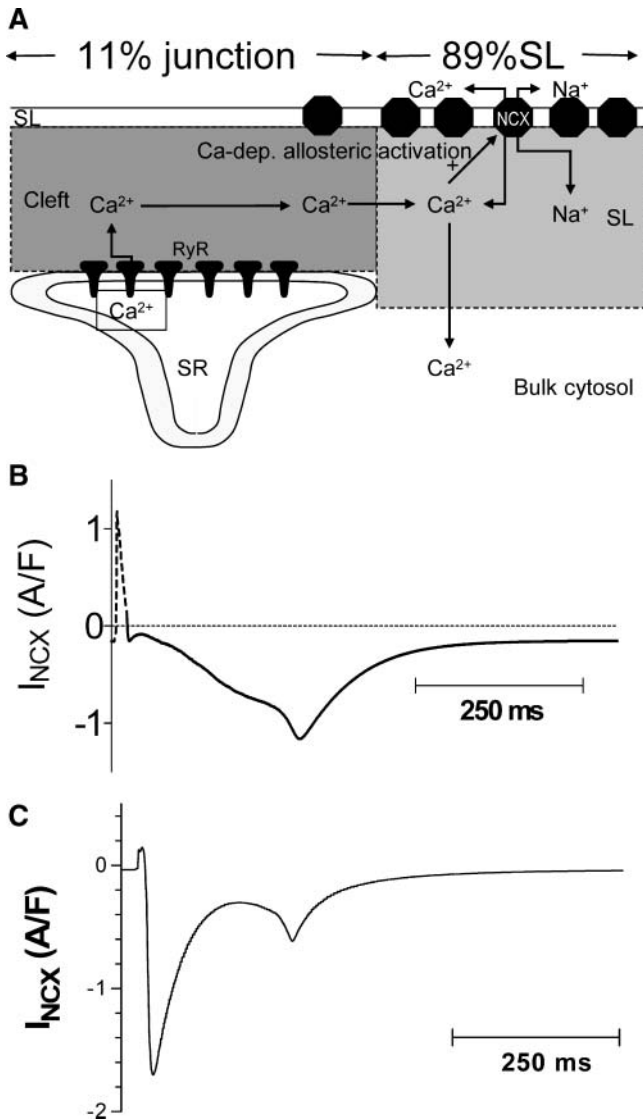
FIGURE 7 (*A*) Diagram illustrating the operation of Na-Ca exchange within the model. The exchanger includes an allosteric Ca-dependent activation (Hilgemann et al., 1992; Weber et al., 2001). (*B*) Model exchange current during an AP (*bottom*). The data of Weber et al. (2002) are shown for comparison (*top*).

Fig. 8 and the model simulates this data quite well. The data indicate that the transport of Ca from the SL and bulk cytosolic compartments is correctly balanced and therefore imply that the balance during ECC and release at steady state is also correct. Note that these integrated steady-state Ca fluxes during a twitch also define the gain of ECC (integrated Ca released/integrated Ca influx) in rabbit during an action potential as 3–4, consistent with cellular data.

Thus, the digital cell can be stimulated to release Ca at normal frequencies to a steady state with characteristics consistent with the cellular physiology observed in vivo. The model is stable (the authors have not found a time limit) and the steady state is dependent strictly upon the parameters of the relevant physiological processes. For instance, as shown

in Fig. 9, a sudden step increase in $[Ca]_{SRT}$ results in an increased release at the next beat. These transients gradually decrease in magnitude returning to exactly the steady state that existed before the step increase. The extra bolus of Ca is, of course, extruded from the cell. The opposite response takes place upon a step decrease in $[Ca]_{SRT}$. Both traces return to the same natural steady state that is not dependent upon the model's history.

This ability to return to steady state is notable. It is a major reason for the model's stability and, to an extent, explains some of its physiological behavior. A change to the environment in which the digital cell operates initiates a series of relevant operational adjustments in all components of the model. These result in a new steady state that, within the bounds of the formulation, is physiologically relevant. In other words, feedback loops that keep the normal cell from becoming unstable are reflected in the model (Overend et al., 1998; Eisner et al., 1998; Trafford et al., 1998).

The physiological utility of the model was tested by simulating well-known cellular responses. The first of these was the phenomenon known as rest decay (Fig. 11 *A*; Bers et al., 1993). The cell was stimulated to steady state and then stimulations were suddenly terminated. Upon resting the cell, the SR lost Ca at a rate comparable with that seen in normal rabbit myocytes. Moreover the decline in amplitude of postrest twitch Ca transients also matched rest-decay data (Fig. 11 *B*). The larger percent decline in twitch $\Delta[Ca]_i$ as a function of $[Ca]_{SRT}$ is a consequence, at least in part, of the steep lumenal Ca dependence of the RyR gating (Fig. 5). Note well that because this relationship levels off before it reaches 0 SR Ca, the SR does not completely drain. Similar to the resting rabbit ventricular myocyte, the resting digital cell has Ca available for release.

The model was further tested by applying different frequencies to simulate the positive force-frequency relationship (Fig. 10 *A*). Force development depends upon $[Ca]_i$ and physiologically the Ca transient amplitude is the major factor that drives its development. We have, therefore, characterized the Ca transient magnitude as an indication of the extent of force developed within the model.

The cell was stimulated to steady state at a low frequency (0.125 Hz). Upon increasing the rate to 0.5 Hz, the transients increased in magnitude until a new steady state was reached. Upon decreasing the frequency, the transients fell back to the initial steady state. Thus a normal force-frequency relationship is implied and the full relationship agrees well with experimental data (Fig. 10 *B*). The inset in the bottom panel of Fig. 10 *B* also shows the rise in diastolic Na in the bulk cytosolic space that takes place as frequency is increased in the model. This rise in Na results from the increased integrated Na entry over time as the number of depolarizations per second is increased. The rise in Na tends to limit Na-Ca exchange activity, thus contributing to the rise in cellular Ca, particularly that within the SR.
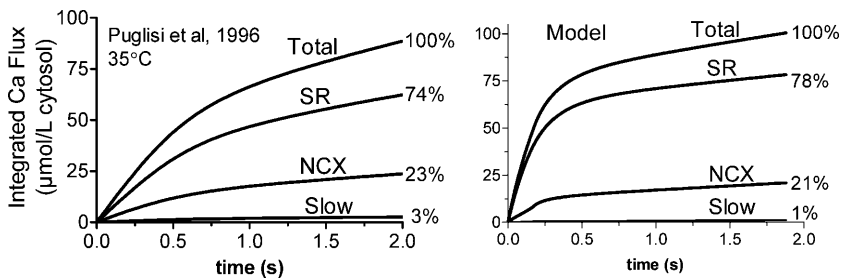
FIGURE 8 The balance of fluxes that transport Ca from the cytosol. Each transporter competes for Ca resulting in a defined percentage of the total Ca translocated by each. The data of Puglisi et al. (1996) are provided for comparison (*left*). The τ of [Ca] decline for the model experiments (190 ms normal twitch, 750 caffeine alone, and 7000 for 0 Na/0 Ca plus caffeine) were similar to the experimentally obtained values there.

DISCUSSION

This article describes a new model that describes the Ca dynamics within the cardiac myocyte. The model was designed to be simple yet descriptive enough to simulate complex physiological responses.

CICR

The goals of the project included the use of CICR to initiate and control SR Ca release while keeping the model available for use on a personal desktop computer with reasonable computational power. This was done by avoiding computationally expensive formulations that include extensive, spatially descriptive, local junctional, control and/or Monte

FIGURE 9 Response to a sudden increase (*red*) or decrease (*blue*) in $[Ca]_{SRT}$ (*bottom*). The model reacts by increasing the release from the SR, thus increasing the peak of the bulk Ca transient (*top*) and decreasing the $[Ca]_{SRT}$ for the next beat until the SR Ca content returns to normal and the model returns to the previous steady state.

Carlo simulations of stochastic RyR properties. The model uses a ''bulk'' junctional compartment that is a small but realistic proportion of the total cell volume (<0.1%). The gating of the SR Ca release channels is graded (Fig. 5) and dependent entirely upon the [Ca] within this cleft (with important modulation of that dependence by $[Ca]_{SR}$). This makes the entire process of ECC more realistic and enables more effective investigation of phenomena that affect CICR.

Although the simplified control via CICR is quite good, the description in this model is still limited. For instance, SR Ca release as a function of voltage has been shown in the elegant experiments of Sipido, Balke, and Weir (Sipido and Wier, 1991; Balke et al., 1994) to have a peak that is slightly shifted to the left of that of the bulk L-type Ca current. The model as it is currently formulated does not include this characteristic. Neither this model, nor any model that lacks the necessary spacial resolution within the cleft is likely to describe such a characteristic accurately.

The RyR is modeled with a modification of the scheme best described by Stern et al. (1999) (Fig. 4). The scheme works remarkably well as described with few changes in the parameters they used. The peak open probability of ≈1% is reasonable when data from the literature are considered. There are 1.5 million RyR per myocyte (Bers and Stiffel, 1993; Bers, 2001). For a single RyR flux of 0.4 pA (Majia-Alvarez et al., 1999) and a peak SR Ca release flux of 2 mM/s, only ~2% of the RyR would be open.

Importantly, however, we have added dependence of those parameters upon $[Ca]_{SR}$ (Fig. 4). Regulation of SR Ca release by SR Ca is well documented (Bassani, J. W. M. et al., 1995a; Janczewski et al., 1995; Eisner et al., 1998; Lukyanenko et al., 1999; Shannon et al., 2002) and may be mediated by a lumenal Ca sensor (Györke and Györke, 1998; Györke et al., 2004).

As formulated, the $[Ca]_{SR}$ affects the RyR in a classic Michaelis-type relationship (Eq. 99). Lower $[Ca]_{SR}$ does not directly inactivate the RyR. Instead, lumenal Ca alters the Ca binding parameters on the cytosolic side of the membrane such that both the lumenal and junctional [Ca] act in combination to both initiate and terminate SR Ca release. The model accounts for the dependence of the ECC process upon SR Ca load largely because of this modification (Fig. 5). Notably it explains the failure of CICR when $[Ca]_{SR}$ is <40–50% of its normal value (Bassani, J. W. M. et al., 1995a; Shannon et al., 2000). It also explains experimental
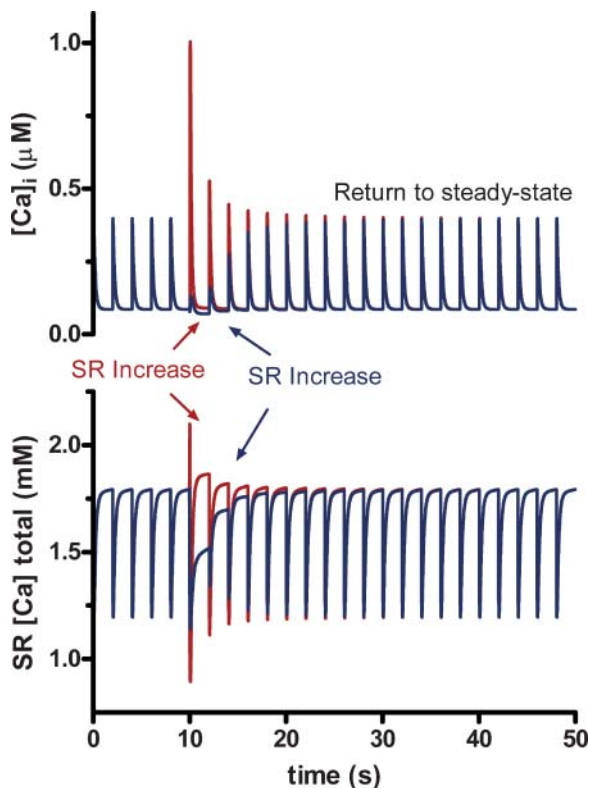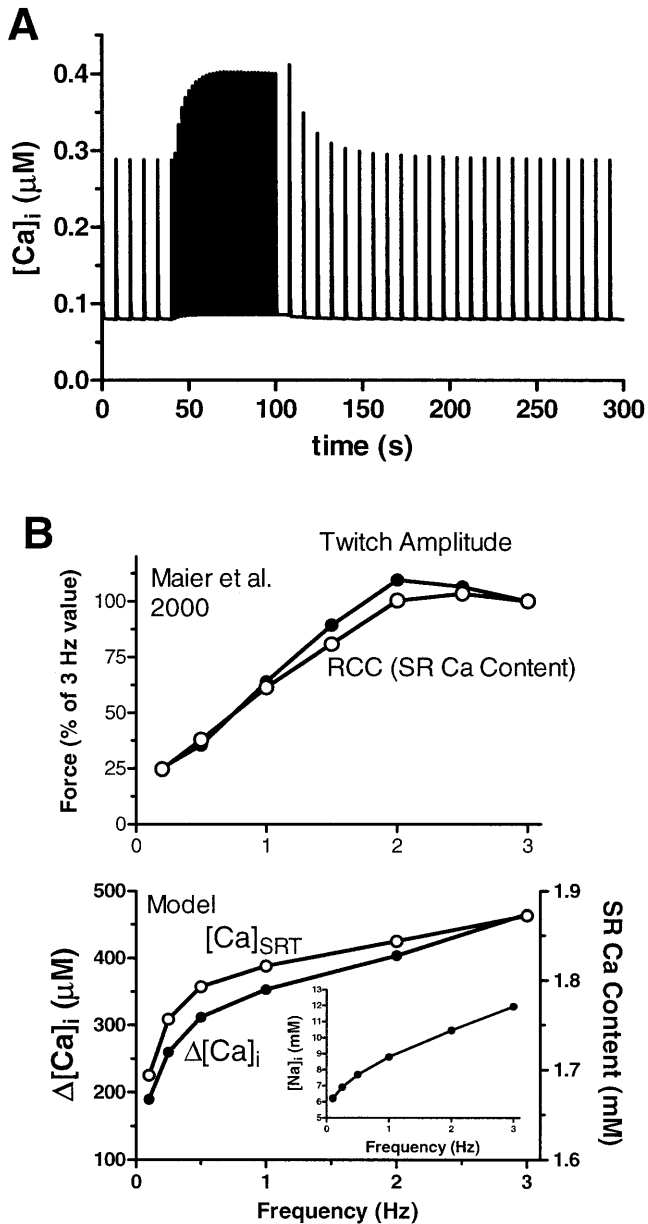
FIGURE 10 The model exhibits a positive force-frequency relationship in response to an increase in frequency from 0.125 to 0.5 Hz (*A*). Panel *B* shows summary data from the model (*bottom*) along with the corresponding rise in diastolic Na concentration in the bulk cytosol (*inset*). Data from Maier et al. (2000) are shown for comparison.

data that have led to conclusions that lumenal Ca depletion plays a key role in the termination of release, not by exhausting the Ca gradient per se, but rather by an allosteric regulatory effect. This extends the list of possible mechanisms for interruption of positive feedback of CICR that were considered by Stern et al. (1999).

Ca transporters

Four Ca transport systems can compete for Ca during Ca transient decline: i), SR Ca ATPase; ii), SL Na-Ca exchange;

iii), SL Ca ATPase; and iv), mitochondrial Ca uptake. The first three are well described in the model whereas the last (which is minor) will be added at a future date.

The Na-Ca exchanger undergoes activation upon Ca binding to an allosteric site located on the exchanger on the intracellular side of the SL membrane (Hilgemann et al., 1992; Matsuoka et al., 1995; Trafford et al., 1995; Weber et al., 2001, 2002). This site has been shown to be physiologically relevant with measurements of the K_d for Ca varying from 125 to 450 nM (Weber et al., 2001).

The new formulation of the Na-Ca exchanger is based upon that in Weber et al. (2001, 2002), which matched extensive data therein. Importantly, the equation accounts for the deactivation of Na-Ca exchange that takes place during the Ca transient as $[Ca]_i$ (and $[Ca]_{SL}$) falls to rest and Ca dissociates from its allosteric activation site. The addition is a double-edged sword. It allows the Na-Ca exchanger to turn off near resting $[Ca]_i$, preventing the high rate of Ca loss that would otherwise continue, making diastolic $[Ca]_i$ too low, and depleting the cell of Ca, yet allows for rest decay (Fig. 10; Bers, 1985; Dani et al., 1979; McCall et al., 1996; Satoh et al., 1997; Terracciano et al., 1995). However, this allosteric Ca-dependent activation is also responsible for a higher than experimentally assessed initial peak in inward Na-Ca exchange current (Fig. 7 *B*; Weber et al., 2001) that corresponds to the peak of the Ca transient in the junction and along the SL. Ongoing investigation into the time dependence of this activation may yield valuable results that may explain this apparent dichotomy and allow a more accurate simulation of the Na-Ca exchange current in the future.

Additionally, unlike some previous formulations (Luo and Rudy, 1994a), the equation also accounts for the effects of intracellular [Na], which is often reduced or removed experimentally to alter the exchange activity. In addition, $[Na]_i$ is known to change within the myocyte during changes in frequency and under the condition of chronic heart failure (Despa et al., 2002b), and this surely is a factor contributing to the force-frequency relationship as shown in the inset of the bottom panel of Fig. 10 *B*. Na also rises in the other compartments to a similar extent. Future studies both in the model as well as at the bench should provide useful quantitative information about the behavior of this important ion.

The SR Ca pump has also been reformulated in a more realistic way. This ATPase is traditionally represented in a unidirectional Hill-type relationship (Sipido and Wier, 1991; Luo and Rudy, 1994a,b; Balke et al., 1994; Bassani et al., 1994). However, it is well known that the pump is a reversible enzyme being capable of mediating both forward and reverse unidirectional fluxes, although the net rate never reverses physiologically (Weber et al., 1966; Makinose, 1971; Takenaka et al., 1982; Feher, 1984; Shannon et al., 2000b, 2001). The extent that the reverse flux takes place to slow uptake under physiological conditions is debatable but by using a formulation that allows for this reversal flux, we have allowed for these potential effects. This representation
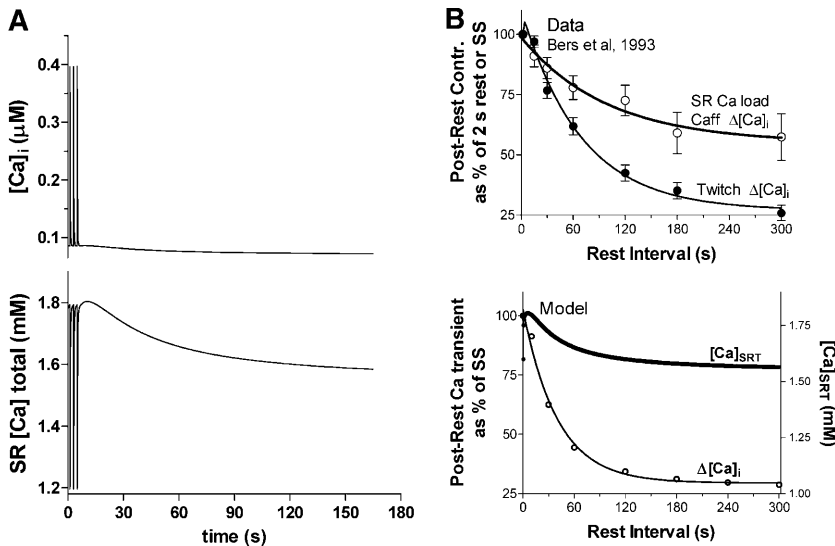
FIGURE 11 The model exhibits normal rest decay (*A*). Summary data for both $[Ca]_{SRT}$ and twitch $\Delta[Ca]_i$ from the model (*bottom*) are to be compared with the data of Bers et al. (1993) (*top*).

will also allow for realistic extension of the model into energetics and ATP consumption because net ATP hydrolysis is reduced, when compared to a simpler pump-leak balance.

Critical to the process of SR Ca uptake was the necessity of formulating a correct balance between the SR Ca pump and the leak of Ca from the organelle. The proper quantity of leak was formulated through the combination of RyR flux plus a passive leak for Ca from the SR into the junctional space. The background leak of Ca from the SR of 3 μM/s at normal $[Ca]_{SRT}$ increased the diastolic value of $[Ca]_{jct}$ and thus sustained an increase in the diastolic RyR activity that added an additional 1 μM/s of leak to total 4 μM/s SR Ca leak. This value is within the normal range (Fig. 4 *B*; *inset*, Györke et al., 1997; Shannon et al., 2001, 2003b). This leak was important in contributing to both the positive force-frequency relationship and rest decay.

Perhaps the most important aspect of the Ca transport is the balance of fluxes (Fig. 8). Bassani et al. (1992) initially described the competition between the relevant transporters for Ca during transient decline. The effectiveness of each of these transporters in this competition varies with species but the human is most like the rabbit, which is described here (Bassani et al., 1993b, 1994; Bassani, R. A. et al., 1995; Negretti et al., 1993; Bers, 2001; Piacentino et al., 2003).

The model is formulated to maintain this balance of fluxes. Of the four relevant transporters only the mitochondrial uptake, a relatively minor flux, is missing. This SL Ca pump transport in the model represents the ''slow'' transport component typically observed in physiological experiments (Bassani et al., 1993a). The mitochondrial part of this component, ~1% of the total Ca efflux from the cytosol during the transient, is distributed among the three existing model fluxes.

The characterization of the fluxes and maintenance of this balance is absolutely critical to the predictive value of the model. For instance, at steady state the amount of Ca that enters the cell is equal to the amount which leaves. Carried further, this means that the amount of Ca taken up into the SR is equal to the amount of release whereas the amount of Ca transported out of the cell on the SL Ca pump and the Na-Ca exchanger is equal to the amount of influx primarily through the L-type Ca channel (plus a minor contribution from outward Na-Ca exchange current). The balance of fluxes indicates the ''gain'' of ECC as defined by the integrated release divided by the integrated current (i.e., the stimulus of the CICR).

In addition, to extend the simulations into situations where transport of one type is altered, one must predict the extent to which other transporters will compensate. For instance, the balance between these fluxes also varies with pathological conditions such as heart failure (Pogwizd et al., 1999, 2001; O'Rourke et al., 1999; Shannon et al., 2003b), which involves an increase in Na-Ca exchange activity, a decrease in SR Ca pump activity, and an increase in SR Ca leak, depending upon the failure model. The extent to which either or all of these alters $[Ca]_{SRT}$ depends upon the extent to which the alteration of each affects transport relative to the other and the competition among the transporters must be correct to predict the overall effects (Shannon et al., 2003b).

The subsarcolemmal Ca compartment

Important for the development of both this aspect of the model as well as the currents across the sarcolemmal membrane was the addition of a subsarcolemmal compartment. During the twitch Ca transient there are spatial gradients near the SL membrane. These gradients are likely due to diffusion restrictions that are caused by the mitochondria and the paracrystaline array in the bulk cytosol. Ca-dependent proteins that are located in or near the membrane are therefore likely responding to a [Ca] that is very different from that which is measured in the bulk cytosolic compartment. The presence of the SL compartment is also suggested by the

TABLE 1   Abbreviations used in the text

Abbreviation	Definition
Δx_{C1-C2}	Distance from the geometric center of compartment C1 to the center of compartment C2
α_y and β_y	Opening and closing rate constant of gate y, respectively
η	Position of the energy barrier controlling voltage dependence of the Na-Ca exchanger
γ_i	Activity coefficient of ion i
σ	$[Na]_o$-dependence factor for f_{NaK}
τ_y	Time constant of gate y
A_{C1-C2}	Surface area for diffusion from compartment C1 to compartment C2
AP	Action potential
B_{max}	Maximal binding capacity
B_{max-SR}	B_{max} for Ca binding within the SR
CICR	Ca-induced Ca release
$[Ca]_{SR}$	Free SR Ca
$[Ca]_{SRT}$	Total SR Ca
D_{C1-C2}	Coefficient for diffusion from compartment C1 to compartment C2
d and f	Voltage-dependent activation and inactivation gates of I_{Ca}
E_i	Nernst potential for ion i, mV
ECC	Excitation-contraction coupling
F	Faraday constant, 96,000 Coulomb/mol
f_{Ca}	Ca-dependent inactivation gate of I_{Ca}
f_{CaB}	Fraction of Ca-bound Ca-dependent inactivation sites of I_{Ca}
f_{NaK}	Voltage-dependence parameter of I_{NaK}
Fx_j	Fraction of total flux j in the compartment of interest
$\bar{G}_j$	Maximal conductance of flux i
H	Hill coefficient SR Ca pump
H_{Na}	Hill coefficient of Na-Ca exchanger for Na
I_{Ca}	L-type Ca current
I_{Na}	Fast Na current
I_{NCX}	Na-Ca exchange current
I_{NaK}	Na-K pump current
I_{SLCaP}	SL Ca pump current
$\bar{I}_c$	Maximum current through channel c
$[i]_i$	Free cytosolic concentration of ion i
$[i]_{jct}$	Free junctional cleft concentration of i
$[i]_{jctT}$	Total junctional cleft concentration of ion i
$[i]_o$	Free concentration of ion i in extracellular compartment
$[i]_{SL}$	Free concentration of ion i in the subsarcolemmal compartment
$[i]_{SLT}$	Total concentration of i in the subsarcolemmal compartment
$[i]_T$	Total cytosolic concentration of ion i
IP_i	Portion of I_{Ca} that is carried by ion i
J_{pump}	Net SR Ca pump flux
J_{pumpF}	SR Ca pump forward flux
J_{pumpR}	SR Ca pump reverse flux
J_{leak}	SR Ca passive leak flux
$J_{SRCaRel}$	SR Ca release flux
K_a	Ca-dependent Na-Ca exchange activation coefficient
k_{CaSR}	$[Ca]_{SR}$-dependent RyR activation coefficient
K_d	Affinity constant of ligand for ion of interest
K_{d-SR}	K_d for Ca binding within the SR
$k_{im}, k_{om},$ k_{oSRCa}, k_{iSRCa}	Rate transition constants for the RyR (Fig. 4)
k_{iCa}, k_{oCa}	Baseline, non-SR-dependent transition rate constants for the RyR
k_{leak}	SR leak rate constant
K_{mi}	K_m of Na-Ca exchanger for ion i

(continued)

TABLE 1 (*Continued*)

Abbreviation	Definition
K_{mf}	K_m SR Ca pump forward mode
K_{mr}	K_m SR Ca pump reverse mode
k_{on}	On rate for binding
k_{off}	Off rate for binding
k_s	SR Ca release rate constant
k_{sat}	Saturation factor of the Na-Ca exchanger at very negative potentials
$m, h,$ and j	Activation gate, fast inactivation gate, and slow inactivation gate, respectively, of I_{Na}
$Max_{SR}, Min_{SR},$ EC_{50-SR}, H_{SR}	Parameters for $[Ca]_{SR}$-dependent activation of SR Ca release
P_{i1i2}	Permeability of channel to ion $i1$ relative to ion $i2$
Q_{10-J}	Temperature adjustment factor
R	Gas constant, 1.987 calories/mol/K
R_c, X_c, Y_c	Gates of channel c
RyR	Ryanodine receptor
SL	Sarcolemma
SR	Sarcoplasmic reticulum
T	Absolute temperature, K
V	Membrane voltage
V_{max}	V_{max} SR Ca pump
z_i	Valence of ion i

published values for the Ca affinity of membrane-associated Ca-dependent proteins such as the Na-Ca exchanger and the Ca-dependent Cl channel. These are generally lower than would be expected if these proteins were dependent upon the bulk cytosolic Ca, and the SL compartment is needed to appropriately incorporate these proteins into the model. Indeed, it was by measuring Na-Ca exchange activity and $I_{Cl(Ca)}$ that the difference in the concentration near the SL membrane was inferred by Trafford et al. (1995) and estimated by Weber et al. (2002) (Fig. 3). We have simulated the effects of the higher [Ca] near the SL membrane by creating a new compartment that is separate from that of the bulk cytosol. It is perhaps worth emphasizing that the authors are not actually proposing the existence of a new anatomical compartment within the cell. Rather, this change in the model reflects the existence of a functional compartment where a different Ca profile exists. Although the depth of this compartment is somewhat arbitrary, it was chosen to allow for a physiologically relevant diffusion coefficient for Ca between the SL compartment and the bulk (Table 2). The model accurately reflects the Ca changes within this SL compartment and therefore is an advance over previous ventricular models in that it better accounts for the activity not only of the Na-Ca exchanger but of all Ca-dependent SL proteins. These include the SL Ca pump, the Ca-dependent Cl current, and the L-type Ca channels within this compartment (which undergo Ca-dependent inactivation). The addition of this compartment with a [Ca] that is generally higher than the bulk may be important for accurate simulation of such phenomena as delayed after depolarizations, which are often related to Na-Ca exchange-mediated diastolic membrane depolarization (Pogwizd et al., 2001).

Steady-state behavior

The model described here comes to steady state. This simply means that it continues to operate with repetitive stimulation in a realistic manner such that the cell does not gain or lose Ca over time unless the cellular environment changes. Moreover, the characteristics of the model at steady state are consistent with the normal cellular physiology (e.g., the balance of fluxes and the gain are correct). The model is, therefore, appropriate for use in situations where continued operation for long periods is necessary. This ability is necessary to accurately simulate physiological and pathophysiological reactions, both in the laboratory where many experiments are conditioned with a number of stimulations, and as part of the larger, more integrated context of the whole tissue or organism (Usyk and McCulloch, 2003).

Importantly, the steady state that is achieved is independent of the history of the digital cell. After perturbation of cellular ionic concentrations, the model always returns to the same steady state that is dependent strictly upon the state of the individual components of the ECC process and upon the extracellular environment (Fig. 9). Such behavior allows simulation of physiological responses that are certain to depend strictly upon the experimental perturbation with no unrelated artifacts.

The model accurately reproduces several well-known physiological responses that are made possible by this steady-state behavior. In particular, it reproduces the normal increase in Ca transient peak in response to an increase in frequency (Fig. 10).

In conclusion, we have formulated a realistic mathematical model of Ca homeostasis within the cardiac myocyte. This model uses recent advances in the study of cardiac ECC to improve over previously proposed models. It should be useful for simulating a variety of cellular responses that are demonstrable in the laboratory and will allow more in-depth investigation into the mechanisms behind these responses, particularly when actual experimental data are difficult to obtain.

APPENDIX

Environment

All tabulated parameters are for temperature $(T) = 310$ K (37°C).

Temperature

All parameters and fluxes (J) that were made temperature sensitive within the model were multiplied by a proportionality constant (Q_J) such that:

$$Q_J = (Q_{10-J})^{(T-310)/10}, \qquad (8)$$

where the Q_{10} is a constant that represents the change in the relevant parameter for each 10°C change in temperature.

Diffusion

Diffusion is considered to take place, on average, from the center of each compartment to the center of its adjacent compartment. The junctional compartment communicates only with the SL compartment, the SL compartment with the junction and the bulk cytosolic compartments, and the bulk cytosolic compartment only with the SL.

For ion I diffusion over a distance x through area A from the center of compartment C1 to the center of compartment C2 (Table 2):

$$J_{I(C1-C2)} = D_{I(C1-C2)}A\frac{[I]_{C1} - [I]_{C2}}{\Delta x_{C1-C2}}. \qquad (9)$$

Nernst potential

For each compartment C, the Nerst potential E_C is calculated as:

$$E_{Na} = \frac{RT}{F}\ln\frac{[Na]_o}{[Na]_C} \qquad (10)$$

$$E_K = \frac{RT}{F}\ln\frac{[K]_o}{[K]_i} \qquad (11)$$

$$E_{Ca} = \frac{RT}{2F}\ln\frac{[Ca]_o}{[Ca]_C} \qquad (12)$$

$$E_{Cl} = \frac{RT}{F}\ln\frac{[Cl]_i}{Cl_o} \qquad (13)$$

Voltage

Change in voltage was considered to be the result of the sum of all currents across the membrane and no regional variations in voltage were considered.

Na buffering

Significant, rapid Na buffering was only considered to be associated with cell membrane and therefore was only present in the SL and junctional compartments. The change in Na binding to ligand L over time $(d[Na\cdot L]/dt)$ for each compartment was calculated as (Table 3):

$$d\frac{[Na \cdot L]}{dt} = k_{on}[Na](B_{max} - [Na \cdot L]) - k_{off}[Na \cdot L] \qquad (14)$$

TABLE 2 Environmental parameters

Parameter	Value	Units
Cell length	100	μm
Cell radius	10.25	μm
Junction radius	160	nm
Junction depth	15	nm
SL depth	45	nm
$A_{junction-SL}$	3.01×10^{-6}	cm^2
$A_{SL-cytosol}$	1.30×10^{-4}	cm^2
$D_{Ca(junctiontoSL)}$	1.64×10^{-6}	cm^{2}s^{-1}
$D_{Ca(SL-cytosol)}$	1.22×10^{-6}	cm^{2}s^{-1}
$D_{Na(junction-SL)}$	1.09×10^{-5}	cm^{2}s^{-1}
$D_{Na(SL-cytosol)}$	1.79×10^{-5}	cm^{2}s^{-1}
$\Delta x_{junction-SL}$	0.5	μm
$\Delta x_{SL-cytosol}$	0.45	μm
$[Cl]_i$	15	mM
$[Cl]_o$	150	mM
$[K]_o$	5.4	mM
$[K]_i$	135	mM
$[Na]_o$	145	mM
$[Ca]_o$	1.8	mM
$[Mg]_i$	1	mM

TABLE 3   Na buffering parameters

Parameter	Value	Units*
K_{on}	0.1	$mM^{-1}s^{-1}$
K_{off}	1	s^{-1}
K_d	10	mM
B_{max} junction	3.7	mM
B_{max} SL	1.65	mM
B_{max} cytosol	0	mM

*All units are mmol/l cytosol. Concentrations in the actual compartments can be calculated assuming 11% of membrane-bound components are in the junctional cleft and 89% are in the SL compartment.

Na currents

Na channels and the Na-K pump were all considered to be evenly distributed throughout the cell membrane. The equations are as in Luo and Rudy (1994a, Table 4). The Nernst potential (E_{Na}) was therefore considered to be the result of the difference between the extracellular compartment and the interior cell compartment under the region of the cell membrane where the channels are present. For instance, junctional Na channels (11% of the total) were dependent upon extracellular [Na] and junctional [Na].

Fast Na current

If $V \geq -40$ mV:

$$\alpha_h = 0 \tag{15}$$

$$\alpha_j = 0 \tag{16}$$

$$\beta_h = \frac{1}{0.13\left(1 + \exp\left(\frac{(V + 10.66)}{-11.1}\right)\right)} \tag{17}$$

$$\beta_j = \frac{0.3 \exp(-2.535 \times 10^{-7} V)}{1 + \exp(-0.1(V + 32))} \tag{18}$$

If $V < -40$ mV

$$\alpha_h = 0.135 \exp\left(\frac{80 + V}{-6.8}\right) \tag{19}$$

TABLE 4   Na transport parameters

Parameter	Value	Units
$\bar{G}_{INa}$	16	$mS/\mu F$
Fx_{Na} junction	0.11	
Fx_{Na} SL	0.89	
$\bar{G}_{NaBk}$	0.297×10^{-3}	$mS/\mu F$
Fx_{NaBk} junction	0.11	
Fx_{NaBk} SL	0.89	
Q_{10-NaK}	1.63	
$\bar{I}_{NaK}$	1.91	A/F
K_{mNai}	11.0	mM
$Q_{10-KmNai}$	1.49	
K_{mKo}	1.5	mM
H_{NaK}	4	
Fx_{NaK} junction	0.11	
Fx_{NaK} SL	0.89	

$$\alpha_m = \frac{0.32(V + 47.13)}{1 - \exp(-0.1(V + 47.13))} \tag{23}$$

$$\beta_m = 0.08 \exp\left(\frac{-V}{11}\right) \tag{24}$$

$$h_\infty = \frac{\alpha_h}{\alpha_h + \beta_h} \tag{25}$$

$$\tau_h = \frac{1}{\alpha_h + \beta_h} \tag{26}$$

$$\frac{dh}{dt} = \frac{h_\infty - h}{\tau_h} \tag{27}$$

$$j_\infty = \alpha_j / (\alpha_j + \beta_j) \tag{28}$$

$$\tau_j = \frac{1}{\alpha_j + \beta_j} \tag{29}$$

$$\frac{dj}{dt} = \frac{j_\infty - j}{\tau_j} \tag{30}$$

$$m_\infty = \frac{\alpha_m}{\alpha_m + \beta_m} \tag{31}$$

$$\alpha_j = \frac{(-1.2714 \times 10^5 \exp(0.2444V) - 3.474 \times 10^{-5} \exp(-0.04391V))(V + 37.78)}{1 + \exp(0.311(V + 79.23))} \tag{20}$$

$$\tau_m = \frac{1}{\alpha_m + \beta_m} \tag{32}$$

$$\beta_h = 3.56 \exp(0.079V) + 3.1 \times 10^5 \exp(0.35V) \tag{21}$$

$$\frac{dm}{dt} = \frac{m_\infty - m}{\tau_m} \tag{33}$$

$$\beta_j = \frac{0.1212[\exp(-0.01052V)]}{1 + \exp(-0.1378(V + 40.14))} \tag{22}$$

If time = 0:

$$h = h_\infty \tag{34}$$

$$j = j_\infty \tag{35}$$

$$m = m_\infty \tag{36}$$

$$I_{Na} = Fx_{Na}\bar{G}_{INa}m^3hj(V - E_{Na}) \tag{37}$$

Na leak current

$$I_{NaBk} = Fx_{NaBk}\bar{G}_{NaBk}(V - E_{Na}) \tag{38}$$

Na-K pump

$$\sigma = \frac{\exp\left(\dfrac{[Na]_o}{67.3}\right) - 1}{7} \tag{39}$$

$$f_{NaK} = \frac{1}{1 + 0.1245\exp\left(-0.1\dfrac{VF}{RT}\right) + 0.0365\sigma\exp\left(\dfrac{-VF}{RT}\right)} \tag{40}$$

$$I_{NaK} = \frac{Fx_{NaK}\,Q_{NaK}\,\bar{I}_{NaK}f_{NaK}[K]_o}{1 + (Q_{KmNai}K_{mNai}/[Na]_1)^H_{NaK}([K]_o + K_{mKo})} \tag{41}$$

K currents

All K channels were considered to be evenly distributed in the cell membrane, and potassium was homogeneous both inside and outside of the cell. Therefore K channels were not compartmentalized and the K currents that were independent of Na and Ca were considered to be the same in all regions of the membrane. All parameters are defined in Table 5.

*I*_{Kr}

$$\bar{G}_{IKr} = 0.03\left(\frac{[K]_o}{5.4}\right)^{0.5} \tag{42}$$

$$X_{r\infty} = \frac{1}{1 + \exp\left(-\dfrac{(V + 50)}{7.5}\right)} \tag{43}$$

$$\tau_{Xr} = \frac{1}{\left(\begin{array}{c} 0.00138(V + 7)/(1 - \exp(-0.123(V + 7))) \\ + 0.00061(V + 10)/(\exp(0.145(V + 10)) - 1) \end{array}\right)} \tag{44}$$

$$R_r = \frac{1}{1 + \exp\left(\dfrac{V + 33}{22.4}\right)} \tag{45}$$

$$\frac{dX_r}{dt} = (X_{r\infty} - X_r)/\tau_{Xr} \tag{46}$$

If time = 0:

$$X_r = X_{r\infty} \tag{47}$$

$$I_{Kr} = \bar{G}_{IKr}X_rR_r(V - E_K) \tag{48}$$

*I*_{Ks}

I_{Ks} was evenly distributed throughout the cell membrane and current was dependent upon the [Na] under the membrane compartment in which the channels are located. For instance, I_{Ks} channels located within the junctional compartment were dependent upon junctional [Na].

$$pCai = -\log([Ca]_i + 3) \tag{49}$$

$$\bar{G}_{Ks} = 0.07\left(0.057 + \frac{0.19}{(1 + \exp(-7.2 + (pCai/0.6)))}\right) \tag{50}$$

$$\tag{51}$$

For the compartment, C, in which the channels are located:

$$E_{Ks} = \frac{RT}{F}\ln\left(\frac{[K]_o + P_{NaK}[Na]_o}{[K]_i + P_{NaK}[Na]_C}\right) \tag{52}$$

$$X_{s\infty} = \frac{1}{1 + \exp\left(-\dfrac{V - 1.5}{16.7}\right)} \tag{53}$$

$$\tau_{Xs} = \frac{1}{\left(\dfrac{7.19 \times 10^{-5}(V + 30)}{1 - \exp(-0.148(V + 30))}\right) + \left(\dfrac{1.31 \times 10^{-4}(V + 30)}{(-1 + \exp(0.0687(V + 30)))}\right)} \tag{54}$$

$$\frac{dX_s}{dt} = \frac{X_{s\infty} - X_s}{\tau_{Xs}} \tag{55}$$

If time = 0:

$$X_s = X_{s\infty} \tag{56}$$

$$I_{Ks} = Fx_{Ks}\bar{G}_{Ks}X_s^2(V - E_{Ks}) \tag{57}$$

TABLE 5   K current parameters

Parameter	Value	Units
$G_{to,s}$	0.02	mS/μF
$G_{to,f}$	0.06	mS/μF
P_{NaK}	0.01833	
Fx_{Ks} junction	0.11	
Fx_{Ks} SL	0.89	

I_{to}

$I_{to,s}$

$$X_{to,s-\infty} = 1.0/(1.0 + \exp(-(V + 3.0)/15.0)) \quad (58)$$

$$Y_{to,s-\infty} = 1.0/(1.0 + \exp((V + 33.5)/10.0)) \quad (59)$$

$$R_{s-\infty} = 1.0/(1.0 + \exp((V + 33.5)/10.0)) \quad (60)$$

$$\tau_{Xto,s} = 9.0/(1.0 + \exp((V + 3.0)/15.0)) + 0.5 \quad (61)$$

$$\tau_{Yto,s} = 3000.0/(1.0 + \exp((V + 60.0)/10.0)) + 30.0 \quad (62)$$

$$I_{to,s} = G_{to,s}X_{to,s}(Y_{to,s} + 0.5R_{s-\infty})(V - E_K) \quad (63)$$

$I_{to,f}$

$$X_{to,f-\infty} = 1.0/(1.0 + \exp(-(V + 3.0)/15.0)) \quad (64)$$

$$Y_{to,f-\infty} = 1.0/(1.0 + \exp((V + 33.5)/10.0)) \quad (65)$$

$$\tau_{Xto,f} = 3.5[exp(-1.0(V/30.0)(V/30.0))] + 1.5 \quad (66)$$

$$\tau_{Yto,f} = 20.0/(1.0 + \exp((V + 33.5)/10.0)) + 20.0 \quad (67)$$

$$I_{to,f} = G_{to,f}(X_{to,f})Y_{to,f}(V - E_K) \quad (68)$$

I_{K1}

$$\bar{G}_{K1} = 0.9\left(\frac{[K]_o}{5.4}\right)^{0.5} \quad (69)$$

$$\alpha_{K1} = \frac{1.02}{1 + \exp(0.2385(V - E_K - 59.215))} \quad (70)$$

$$\beta_{K1} = \frac{0.49124\exp(0.08032(V - E_K + 5.476)) + \exp(0.06175(V - E_K - 594.31))}{1 + \exp(-0.5143(V - E_K + 4.753))} \quad (71)$$

$$K1_\infty = \frac{\alpha_{K1}}{\alpha_{K1} + \beta_{K1}} \quad (72)$$

$$I_{K1} = \bar{G}_{K1}K1_\infty(V - E_K) \quad (73)$$

$I_{Cl(Ca)}$

$I_{Cl(Ca)}$ was considered to be evenly distributed throughout the cell membrane and was dependent upon the [Ca] in the compartment just under the portion of the membrane in which the channels were located. For each compartment, C (Table 6):

TABLE 6 Ca-dependent Cl current parameters

Parameter	Value	Units
$\bar{G}_{Cl}$	0.109625	mS/μF
$\bar{G}_{Clbk}$	0.009	mS/μF
K_{dClCa}	100	μM
Fx_{Cl} junction	0.11	
Fx_{Cl} SL	0.89	

$$I_{Cl} = Fx_{Cl}\frac{\bar{G}_{Cl}(V - E_{Cl})}{1 + \frac{K_{dClCa}}{[Ca]_C}} \quad (74)$$

I_{Clbk}

I_{Clbk} (background SL Cl flux Table 6) was considered to be evenly distributed throughout the cell membrane.

$$I_{Clbk} = \bar{G}_{Clbk}(V - E_{Cl}) \quad (75)$$

Ca buffering

Ca buffering parameters are as defined in Table 7.

$$d\frac{[Ca \cdot L]}{dt} = k_{on}[Ca](B_{max} - [Ca \cdot L]) - k_{off}[Ca \cdot L] \quad (76)$$

Ca currents

L-type Ca current

L-type Ca channels were concentrated within the junctional membrane such that 90% of the total number are located there. The formulation is based in the Goldman-Hodgkin-Katz equation and the channel was considered to be permeant to Ca, Na, and K. Total L-type current was the sum of the Ca, Na, and K currents. For compartment C (Table 8):

$$f_{Ca} = 1 - f_{CaB} \quad (77)$$

$$\frac{df_{CaB}}{dt} = 1.7[Ca]_C(1 - f_{CaB}) - 11.9 f_{CaB} \quad (78)$$

$$d_\infty = 1/(1 + \exp(-(V + 14.5)/6.0)) \quad (79)$$

$$\tau_d = d_\infty\frac{1 - \exp\left(\frac{-(V + 14.5)}{6.0}\right)}{0.035(V + 14.5)} \quad (80)$$

$$f_\infty = \frac{1}{1 + \exp\left(\frac{(V + 35.06)}{3.6}\right)} + \frac{0.6}{1 + \exp\left(\frac{(50 - V)}{20}\right)} \quad (81)$$

TABLE 7 Parameters for Ca buffers

Buffer	Compartment	B_{max} (μmol/l cytosol*)	K_d (μM)	k_{off} (s^{-1})	k_{on} (μM^{-1}s^{-1})
Troponin C	Cytosol	70	0.6	19.6	32.7
Troponin C Ca-Mg (Ca)	Cytosol	140	0.0135	0.032	2.37
Troponin C Ca-Mg (Mg)	Cytosol	140	1111	3.33	0.003
Calmodulin	Cytosol	24	7	238	34
Myosin (Ca)	Cytosol	140	0.0333	0.46	13.8
Myosin (Mg)	Cytosol	140	3.64	0.057	0.0157
SR	Cytosol	19	0.6	60	100
SL	SL	37.4	13	1300	100
SL	Junction	4.6	13	1300	100
SLHigh	SL	13.4	0.3	30	100
SLHigh	Junction	1.65	0.3	30	100
Indo-1	Cytosol	25	0.6	60	100
Indo-1	SL	0.77	0.6	60	100
Indo-1	Junction	0.02	0.6	60	100
Fluo-3	Cytosol	25	1.1	110	100
Fluo-3	SL	0.77	1.1	110	100
Fluo-3	Junction	0.02	1.1	110	100
Calsequestrin	SR	140	650	65,000	100

*Concentrations in the actual compartments can be calculated assuming 11% of membrane-bound components are in the junctional cleft and 89% are in the SL compartment.

$$\tau_f = \frac{1}{(0.0197[\exp(-(0.0337(V + 14.5))^2)]) + 0.02} \quad (82)$$

$$\alpha_d = \frac{d_\infty}{\tau_d} \quad (83)$$

$$\beta_d = \frac{1 - d_\infty}{\tau_d} \quad (84)$$

$$\alpha_f = \frac{f_\infty}{\tau_f} \quad (85)$$

$$\beta_f = \frac{1 - f_\infty}{\tau_f} \quad (86)$$

$$\frac{dd}{dt} = \frac{d_\infty - d}{\tau_d} \quad (87)$$

$$\frac{df}{dt} = \frac{f_\infty - f}{\tau_f}, \quad (88)$$

if time = 0 then:

$$d = d_\infty \quad (89)$$

$$f = f_\infty \quad (90)$$

where S is Ca, Na, or K for the relevant compartment:

$$\bar{I}_S = P_S z_s^2 V \frac{F^2}{RT} \frac{\gamma_{Si}[S]_{SL}\exp\left(\frac{z_s VF}{RT}\right) - \gamma_{So}[S]_o}{\exp\left(\frac{z_s VF}{RT}\right) - 1} \quad (91)$$

$$IP_S = d(f)f_{Ca}Q_{CaL}\bar{I}_S \quad (92)$$

$$I_{CaL} = Fx_{CaL}(IP_{Ca} + IP_{Na} + IP_K) \quad (93)$$

TABLE 8 Ca current parameters

Parameter	Value	Units
Fx_{CaL} junction	0.9	
Fx_{CaL} SL fraction	0.1	
P_{Ca}	5.4×10^{-4}	cm/s
γ_{Cai}	0.341	
γ_{Cao}	0.341	
P_{Na}	1.5×10^{-8}	cm/s
γ_{Nai}	0.75	
γ_{Nao}	0.75	
P_K	2.7×10^{-7}	cm/s
γ_{Ki}	0.75	
γ_{Ko}	0.75	
Q_{10-CaL}	1.8	
$\bar{G}_{CaBk}$	0.0002513	mS/μF
Fx_{CaBk} junction	0.11	
Fx_{CaBk} SL fraction	0.89	

SL Ca leak

I_{CaBk} (background SL Ca flux) was distributed evenly throughout the cell membrane. For each compartment (Table 8):

$$I_{CaBk} = Fx_{CaBk}\bar{G}_{CaBk}(V - E_{Ca}) \quad (94)$$

SL Ca transport

All SL transport proteins were considered to be evenly distributed across the membrane with 11% in the junctional cleft and 89% in the SL compartment.

Na-Ca exchange

The Na-Ca exchange equation is essentially as in Weber et al. (2001). The equation assumes a ping-pong bi-bi mechanism and accounts for the Na

and Ca concentrations on both sides of the membrane (Segal, 1993). The terms that describe the voltage dependence are essentially as described in Luo and Rudy (1994a). The temperature dependence (i.e., the Q_{10}) is as described in Puglisi et al. (1999). For each compartment C (Table 9):

$$K_{a} = \frac{1}{1 + \left(\frac{K_{d-Act}}{[Ca]_{C}}\right)^{3}} \quad (95)$$

$$I_{NCX} = \frac{K_{a}Q_{NCX}V_{max}\left(\exp(\frac{\eta VF}{RT})[Na]_{C}^{H_{Na}}[Ca]_{o} - \exp(\frac{(\eta-1)VF}{RT})[Na]_{o}^{H_{Na}}[Ca]_{C}\right)}{\left(\begin{array}{c} K_{mCai}[Na]_{o}^{H_{Na}}(1 + (\frac{[Na]_{C}}{K_{mNai}})^{H_{Na}}) + \\ K_{mNao}^{H_{Na}}[Ca]_{C}(1 + \frac{[Ca]_{C}}{K_{mCai}}) + K_{mCao}[Na]_{C}^{H_{Na}} \\ + [Na]_{C}^{H_{Na}}[Ca]_{o} + [Na]_{o}^{H_{Na}}[Ca]_{C} \end{array}\right)(1 + k_{sat}\exp((\eta-1)\frac{VF}{RT}))}. \quad (96)$$

SL Ca pump

For each compartment C (Table 10):

$$I_{SLCaP} = \frac{Fx_{SLCaP}\,Q_{SLCaP}V_{max}}{1 + \left(\frac{K_{m}}{[Ca]_{C}}\right)^{H}} \quad (97)$$

The temperature dependence (i.e., the Q_{10}) is as described in Puglisi et al. (1999).

SR Ca fluxes

SR Ca pump

The SR Ca pump is found only in the cytosolic (i.e., nonjunctional) portion of the membrane that accounts for 90% of the total. The Q_{10} is as described by Puglisi et al. (1999). The equation itself accounts for [Ca] on both sides of the SR membrane and is essentially as described in Segal (1976) and applied in Shannon et al. (2000a, Table 11).

$$J_{SRCaP} = Q_{10-SRCaP}\frac{V_{max}\left(\frac{[Ca]_{i}}{K_{mf}}\right)^{H} - V_{max}\left(\frac{[Ca]_{SR}}{K_{mr}}\right)^{H}}{1 + \left(\frac{[Ca]_{i}}{K_{mf}}\right)^{H} + \left(\frac{[Ca]_{SR}}{K_{mr}}\right)^{H}}. \quad (98)$$

SR Ca release

The SR Ca release channel was model essentially as described in Stern et al. (1999) with an added lumenal $[Ca]_{SR}$ dependence (see Methods, Table 12).

TABLE 9   Na-Ca exchange parameters

Parameter	Value	Units
V_{max}	9.0	A/F
K_{mCai}	3.59	μM
K_{mCao}	1.3	mM
K_{mNai}	12.29	mM
K_{mNao}	87.5	mM
k_{sat}	0.27	
η	0.35	
K_{d-Act}	0.256	μM
H_{Na}	3	
Q_{10-NCX}	1.57	

TABLE 10   SL Ca pump parameters

Parameter	Value	Units
Fx_{SLCaP} junction	0.11	
Fx_{SLCaP} SL	0.89	
V_{max}	2.2	μmol/l cytosol/s
K_{m}	0.5	μM
H	1.6	
$Q_{10-SLCaP}$	2.35	

The channel is located only in the junctional cleft that accounts for 10% of the total SR membrane.

$$k_{CaSR} = Max_{SR} - \frac{Max_{SR} - Min_{SR}}{1 + \left(\frac{EC_{50-SR}}{[Ca]_{SR}}\right)^{H_{SR}}} \quad (99)$$

where k_{oSRCa} and k_{iSRCa} are not diffusion limited:

$$k_{oSRCa} = \frac{k_{oCa}}{k_{CaSR}} \quad (100)$$

$$k_{iSRCa} = k_{iCa}k_{CaSR} \quad (101)$$

$$\frac{dR}{dt} = (k_{im}RI - k_{iSRCa}[Ca]_{jct}R) - (k_{oSRCa}[Ca]_{jct}^{2}R - k_{om}O) \quad (102)$$

$$\frac{dO}{dt} = (k_{oSRCa}[Ca]_{jct}^{2}R - k_{om}O) - (k_{iSRCa}[Ca]_{jct}O - k_{im}I) \quad (103)$$

$$\frac{dI}{dt} = (k_{iSRCa}[Ca]_{jct}O - k_{im}I) - (k_{om}I - k_{oSRCa}[Ca]_{jct}^{2}RI) \quad (104)$$

$$\frac{dRI}{dt} = (k_{om}I - k_{oSRCa}[Ca]_{jct}^{2}RI) - (k_{im}RI - k_{iSRCa}[Ca]_{jct}R) \quad (105)$$

$$J_{SRCaRel} = k_{s}O([Ca]_{SR} - [Ca]_{jct}) \quad (106)$$

The resulting flux is in mmol/l SR/ms.

Passive SR Ca leak

Passive leak was modeled as a gradient-dependent Ca specific channel in the SR membrane (Table 12). It was located only in the junctional cleft and its conductance was adjusted such that the total leak (RyR-dependent and passive) equaled approximately that of Shannon et al. (2002) at 0.5-Hz pacing.

TABLE 11   SR Ca pump parameters

Parameter	Value	Units
V_{max}	286	μmol/l cytosol/s
K_{mf}	0.246	μM
K_{mr}	1.7	mM
H	1.787	
$Q_{10-SRCaP}$	2.6	

TABLE 12 Parameters for SR Ca release

Parameter	Value	Units
k_s	25	ms^{-1}
k_{oCa}	10	$mM^{-2}ms^{-1}$
k_{om}	0.06	ms^{-1}
k_{iCa}	0.5	$mM^{-1}ms^{-1}$
k_{im}	0.005	ms^{-1}
EC_{50-SR}	0.45	mM
Max_{SR}	15	
Min_{SR}	1	
H_{SR}	2.5	
K_{SRleak}	5.348×10^{-6}	ms^{-1}

$$J_{SRLeak} = K_{SRleak}([Ca]_{SR} - [Ca]_{jct}) \qquad (107)$$

The resulting flux is in μmol/l cytosol/s. This flux plus the diastolic release is the total diastolic leak rate.

REFERENCES

Balke, C. W., T. M. Egan, and W. G. Wier. 1994. Processes that remove calcium from the cytoplasm during excitation-contraction coupling in intact rat heart cells. *J. Physiol.* 474:447–462.

Bassani, J. W. M., R. A. Bassani, and D. M. Bers. 1993a. Ca^{2+} cycling between sarcoplasmic reticulum and mitochondria in rabbit cardiac myocytes. *J. Physiol.* 460:603–621.

Bassani, J. W. M., R. A. Bassani, and D. M. Bers. 1993b. Twitch-dependent SR Ca accumulation and release in rabbit ventricular myocytes. *Am. J. Physiol.* 265:C533–C540.

Bassani, J. W. M., R. A. Bassani, and D. M. Bers. 1994. Relaxation in rabbit and rat cardiac cells: species-dependent differences in cellular mechanisms. *J. Physiol.* 476:279–293.

Bassani, J. W. M., W. Yuan, and D. M. Bers. 1995. Fractional SR Ca release is regulated by trigger Ca and SR Ca content in cardiac myocytes. *Am. J. Physiol.* 268:C1313–C1329.

Bassani, R. A., J. Altamirano, J. L. Puglisi, and D. M. Bers. 2004. Action potential duration determines sarcoplasmic reticulum Ca^{2+} reloading in mammalian ventricular myocytes. *J. Physiol.* 559:593–609.

Bassani, R. A., J. W. M. Bassani, and D. M. Bers. 1992. Mitochondrial and sarcolemmal Ca^{2+} transport reduce [Ca^{2+}]$_i$ during caffeine contractures in rabbit cardiac myocytes. *J. Physiol.* 453:591–608.

Bassani, R. A., J. W. M. Bassani, and D. M. Bers. 1995. Relaxation in ferret ventricular myocytes: role of the sarcolemmal Ca ATPase. *Eur J. Physiol.* 430:573–578.

Bean, B. P. 1989. Classes of calcium channels in vertebrate cells. *Annu. Rev. Physiol.* 51:367–384.

Beeler, G. W., and H. Reuter. 1977. Reconstruction of the action potential of ventricular myocardial fibres. *J. Physiol.* 268:177–210.

Bers, D. M. 1985. Ca influx and sarcoplasmic reticulum Ca release in cardiac muscle activation during postrest recovery. *Am. J. Physiol.* 248:H366–H381.

Bers, D. M. 2001. Excitation-Contraction Coupling and Cardiac Contractile Force, 2nd Ed. Kluwer Academic Publishers, Dordrecht, The Netherlands.

Bers, D. M., L.-A. H. Allen, and Y.-J. Kim. 1986. Calcium binding to cardiac sarcolemmal vesicles: potential role as a modifier of contraction. *Am. J. Physiol.* 251:C861–C871.

Bers, D. M., R. A. Bassani, J. W. Bassani, S. Baudet, and L. V. Hryshko. 1993. Paradoxical twitch potentiation after rest in cardiac muscle: increased fractional release of SR calcium. *J. Mol. Cell. Cardiol.* 25:1047–1057.

Bers, D. M., and V. M. Stiffel. 1993. Ratio of ryanodine to dihydropyridine receptors in cardiac and skeletal muscle and implications for E-C coupling. *Am. J. Physiol.* 264:C1587–C1593.

Bondarenko, V. E., G. P. Szigeti, G. C. Bett, S. J. Kim, and R. L. Rasmusson. 2004. A computer model of the action potential of mouse ventricular myocytes. *Am. J. Physiol.* In press.

Cheng, H., M. B. Cannell, and W. J. Lederer. 1995. Models of Ca^{2+} release channel adaptation. *Science.* 267:2009–2010.

Cheng, H., M. R. Lederer, W. J. Lederer, and M. B. Cannell. 1996. Calcium sparks and [Ca^{2+}]$_i$ waves in cardiac myocytes. *Am. J. Physiol.* 270:C148–C159.

Collier, M. C., P. C. Levesque, J. L. Kenyon, and J. R. Hume. 1996. Unitary Cl$^-$ channels activated by cytoplasmic Ca^{2+} in canine ventricular myocytes. *Circ. Res.* 78:936–944.

Dani, A. M., A. Cittadini, and G. Inesi. 1979. Calcium transport and contractile activity in dissociated mammalian heart cells. *Am. J. Physiol.* 237:C147–C155.

Despa, S., M. Islam, S. Pogwizd, and D. Bers. 2002a. Intracellular and Na(+) pump rate in rat and rabbit ventricular myocytes. *J. Physiol.* 539:133–143.

Despa, S., M. A. Islam, C. R. Weber, S. M. Pogwizd, and D. M. Bers. 2002b. Intracellular Na concentration is elevated in heart failure but Na/K pump function is unchanged. *Circulation.* 105:2543–2548.

Dettbarn, C., and P. Palade. 1997. Ca^{2+} feedback on ''quantal'' Ca^{2+} release involving ryanodine receptors. *Mol. Pharmacol.* 52:1124–1130.

DiFrancesco, D., and D. Noble. 1985. A model of cardiac electrical activity incorporating ionic pumps and concentration changes. *Philos. Trans. R. Soc. Lond. B Biol. Sci.* 307:353–398.

Donoso, P., H. Prieto, and C. Hidalgo. 1995. Luminal calcium regulates calcium release in triads isolated from frog and rabbit skeletal muscle. *Biophys. J.* 68:507–515.

Eisner, D., A. Trafford, M. Diaz, C. Overend, and S. O'Neill. 1998. The control of Ca release from the cardiac sarcoplasmic reticulum: regulation versus autoregulation. *Cardiovasc. Res.* 38:589–604.

Fabiato, A. 1985. Time and calcium dependence of activation and inactivation of calcium-induced release of calcium from the sarcoplasmic reticulum of a skinned canine cardiac Purkinje cell. *J. Gen. Physiol.* 85:247–289.

Feher, J. J. 1984. Unidirectional calcium and nucleotide fluxes in sarcoplasmic reticulum. I. Interpretation of flux ratios for different reaction schemes. *Biophys. J.* 45:1125–1133.

Györke, I., and S. Györke. 1998. Regulation of the cardiac ryanodine receptor channel by luminal Ca^{2+} involves luminal Ca^{2+} sensing sites. *Biophys. J.* 75:2801–2810.

Györke, I., N. Hester, L. R. Jones, and S. Györke. 2004. The role of calsequestrin, triadin, and junctin in conferring cardiac ryanodine receptor responsiveness to luminal calcium. *Biophys. J.* 86:2121–2128.

Györke, S., V. Lukyanenko, and I. Györke. 1997. Dual effects of tetracaine on spontaneous calcium release in rat ventricular myocytes. *J. Physiol.* 500:297–309.

Herrmann-Frank, A., and F. Lehmann-Horn. 1996. Regulation of the purified Ca^{2+} release channel/ryanodine receptor complex of skeletal muscle sarcoplasmic reticulum by lumenal calcium. *Pflugers Arch.* 432:155–157.

Hess, M. L., J. B. Lansman, and R. W. Tsien. 1986. Ca channel selectivity for divalent and monovalent cations. Voltage and concentration dependence of single channel current in ventricular heart cells. *J. Gen. Physiol.* 88:293–319.

Hilgemann, D. W., A. Collins, and S. Matsuoka. 1992. Steady-state and dynamic properties of cardiac sodium-calcium exchange. Secondary modulation by cytoplasmic calcium and ATP. *J. Gen. Physiol.* 100:933–961.

Hüser, J., D. M. Bers, and L. A. Blatter. 1998. Subcellular properties of [Ca²⁺]ᵢ-transients in phospholamban-deficient mouse ventricular cells. *Am. J. Physiol.* 274:H1800–H1811.

Jafri, M. S., J. J. Rice, and R. L. Winslow. 1998. Cardiac Ca²⁺ dynamics: the roles of ryanodine receptor adaptation and sarcoplasmic reticulum load. *Biophys. J.* 74:1296–1304.

Janczewski, A. M., H. A. Spurgeon, M. D. Stern, and E. G. Lakatta. 1995. Effects of sarcoplasmic reticulum Ca²⁺ load on the gain function of Ca²⁺ release by Ca²⁺ current in cardiac cells. *Am. J. Physiol.* 268:H916–H920.

Keizer, J., and L. Levine. 1996. Ryanodine receptor adaptation and Ca²⁺-induced Ca²⁺ release-dependent Ca²⁺ oscillations. *Biophys. J.* 71:3477–3487.

Kurebayashi, N., and Y. Ogawa. 1998. Effect of luminal calcium on Ca²⁺ release channel activity of sarcoplasmic reticulum in situ. *Biophys. J.* 74:1795–1807.

Linz, K. W., and R. Meyer. 1998. Control of L-type calcium current during the action potential of guinea-pig ventricular myocytes. *J. Physiol.* 513:425–442.

Linz, K. W., and R. Meyer. 2000. Profile and kinetics of L-type calcium current during the cardiac ventricular action potential compared in guinea-pigs, rats and rabbits. *Pflugers Arch.* 439:588–599.

Lukyanenko, V., I. Györke, and S. Györke. 1996. Regulation of calcium release by calcium inside the sarcoplasmic reticulum in ventricular myocytes. *Pflugers Arch.* 432:1047–1054.

Lukyanenko, V., D. Subramanian, I. Györke, T. F. Wiesner, and S. Györke. 1999. The role of lumenal Ca²⁺ in the generation of Ca²⁺ waves in rat ventricular myocytes. *J. Physiol.* 518:173–186.

Lukyanenko, V., S. Viatchenko-Karpinski, A. Smirnov, T. F. Wiesner, and S. Györke. 2001. Dynamic regulation of sarcoplasmic reticulum Ca²⁺ content and release by luminal Ca²⁺-sensitive leak in rat ventricular myocytes. *Biophys. J.* 81:785–798.

Luo, C.-H., and Y. Rudy. 1994a. A dynamic model of the cardiac ventricular action potential. I. Simulations of ionic currents and concentration changes. *Circ. Res.* 74:1071–1096.

Luo, C.-H., and Y. Rudy. 1994b. A dynamic model of the cardiac ventricular action potential. II. After depolarizations, triggered activity, and potentiation. *Circ. Res.* 74:1097–1113.

Maier, L. S., D. M. Bers, and B. Pieske. 2000. Differences in Ca²⁺-handling and sarcoplasmic reticulum Ca²⁺-content in isolated rat and rabbit myocardium. *J. Mol. Cell. Cardiol.* 32.

Majia-Alvarez, R., C. Kettlun, E. Rios, M. Stern, and M. Fill. 1999. Unitary Ca²⁺ current through cardiac ryanodine receptor channels under quasi-physiological ionic conditions. *J. Gen. Physiol.* 113:177–186.

Makinose, M. 1971. Calcium efflux dependent formation of ATP from ADP and orthophosphate by the membranes of the sarcoplasmic vesicles. *FEBS Lett.* 12:269–270.

Matsuoka, S., D. A. Nicoll, L. V. Hryshko, D. O. Levitski, J. N. Weiss, and K. D. Philipson. 1995. Regulation of the cardiac Na⁺-Ca²⁺ exchanger by Ca²⁺. *J. Gen. Physiol.* 105:403–420.

McAllister, R. E., D. Noble, and R. W. Tsien. 1975. Reconstruction of the electrical activity of cardiac Purkinje fibres. *J. Physiol.* 251:1–59.

McCall, E., L. V. Hryshko, V. M. Stiffel, D. M. Christensen, and D. M. Bers. 1996. Possible functional linkage between the cardiac dihydropyridine and ryanodine receptor: acceleration of rest decay by Bay K 8644. *J. Mol. Cell. Cardiol.* 28:79–93.

Negretti, N., S. C. O'Neil, and D. A. Eisner. 1993. The effects of inhibitors of sarcoplasmic reticulum function on the systolic Ca²⁺ transient in rat ventricular myocytes. *J. Physiol.* 468:35–52.

Nordin, C. 1993. Computer model of membrane current and intracellular Ca flux in the isolated guinea pig ventricular myocytes. *Am. J. Physiol.* 265:H2117–H2136.

Nuss, H. B., and S. R. Houser. 1993. T-type Ca²⁺ current is expressed in hypertrophied adult feline left ventricular myocytes. *Circ. Res.* 73:777–782.

O'Rourke, B., D. A. Kass, G. F. Tomaselli, S. Kääb, R. Tunin, and E. Marban. 1999. Mechanisms of altered excitation-contraction coupling in

canine tachycardia-induced heart failure. I. Experimental studies. *Circ. Res.* 84:562–570.

Overend, C. L., D. A. Eisner, and S. C. O'Neill. 1998. The effect of tetracaine on stimulated contractions, sarcoplasmic reticulum Ca²⁺ content and membrane current in isolated rat ventricular myocytes. *J. Physiol.* 507:759–769.

Page, E., L. P. Mccallister, and B. Power. 1971. Stereological measurements of cardiac ultrastructures implicated in excitation-contraction coupling. *Proc. Natl. Acad. Sci. USA.* 68:1465–1466.

Page, E., and M. Surdyk-Droske. 1979. Distribution, surface density and membrane area of diadic junctional contacts between plasma membrane and terminal cisterns in mammalian ventricle. *Circ. Res.* 45:260–267.

Pandit, S. V., W. R. Giles, and S. S. Demir. 2003. A mathematical model of the electrophysiological alterations in rat ventricular myocytes in type-I diabetes. *Biophys. J.* 84:832–841.

Peterson, B. Z., C. D. DeMaria, J. P. Adelman, and D. T. Yue. 1999. Calmodulin is the Ca²⁺ sensor for Ca²⁺-dependent inactivation of L-type calcium channels. *Neuron.* 22:549–558.

Piacentino, V., III, C. R. Weber, X. Chen, J. Weisser-Thomas, K. B. Margulies, D. M. Bers, and S. R. Houser. 2003. Cellular basis of abnormal calcium transients of failing human ventricular myocytes. *Circ. Res.* 92:651–658.

Pogwizd, S. M., M. Qi, W. Yuan, A. M. Samarel, and D. M. Bers. 1999. Upregulation of Na⁺/Ca²⁺ exchanger expression and function in an arrhythmogenic rabbit model of heart failure. *Circ. Res.* 85:1009–1019.

Pogwizd, S. M., K. Schlotthauer, L. Li, W. Yuan, and D. M. Bers. 2001. Arrhythmogenesis and contractile dysfunction in heart failure: roles of sodium-calcium exchange, inward rectifier potassium current, and residual beta-adrenergic responsiveness. *Circ. Res.* 88:1095–1096.

Priebe, L., and D. J. Beuckelmann. 1998. Simulation study of cellular electric properties in heart failure. *Circ. Res.* 82:1206–1223.

Puglisi, J. L., A. Bassani, J. Rosana, W. M. Bassani, J. N. Amin, and D. M. Bers. 1996. Temperature and relative contributions of Ca transport systems in cardiac myocyte relaxation. *Am. J. Physiol.* 270:H1772–H1778.

Puglisi, J. L., and D. M. Bers. 2001. LabHEART: an interactive computer model of rabbit venticular myocyte ion channels and Ca transport. *Am. J. Physiol.* 281:C2049–C2060.

Puglisi, J. L., W. Yuan, J. W. M. Bassani, and D. M. Bers. 1999. Ca influx through Ca channels in rabbit ventricular myocytes during action potential clamp: influence of temperature. *Circ. Res.* 85:e7–e16.

Qin, N., R. Olcese, M. Branby, T. Lin, and L. Birnbaumer. 1999. Ca²⁺-induced inhibition of the cardiac Ca²⁺ channel depends on calmodulin. *Proc. Natl. Acad. Sci. USA.* 96:2435–2438.

Salata, J. J., N. K. Juriewicz, B. Jow, K. Folander, P. J. Guinosso, Jr., B. Raynor, R. Swanson, and B. Fermini. 1996. IK of rabbit ventricle is composed of two currents: evidence for IKs. *Am. J. Physiol.* 271:H2477–H2489.

Satoh, H., L. A. Blatter, and D. M. Bers. 1997. Effects of [Ca²⁺]ᵢ, SR Ca²⁺ load, and rest on Ca²⁺ spark frequency in ventricular myocytes. *Am. J. Physiol.* 272:H657–H668.

Satoh, H., L. M. D. Delbridge, L. A. Blatter, and D. M. Bers. 1996. Surface/volume relationship in cardiac myocytes studied with confocal microscopy and membrane capacitance measurements: species-dependence and developmental effects. *Biophys. J.* 70:1494–1504.

Scheifer, A., G. Meissner, and G. Isenberg. 1995. Ca²⁺ activation and Ca²⁺ inactivation of canine reconstituted cardiac sarcoplasmic reticulum Ca²⁺-release channels. *J. Physiol.* 489:337–348.

Scriven, D. R., P. Dan, and E. D. Moore. 2000. Distribution of proteins implicated in excitation-contract coupling in rat ventricular myocytes. *Biophys. J.* 79:2682–2691.

Scriven, D. R. L., A. Klimek, K. L. Lee, and E. D. W. Moore. 2002. The molecular architecture of calcium microdomains in rat cardiomyocytes. *Ann. N. Y. Acad. Sci.* 976:488–499.

Segal, I. H. 1976. Enzymes. *In* Biochemical Calculations. John Wiley and Sons, New York, NY. 220–221.

Segal, I. H. 1993. Steady-state kinetics of multireactant enzymes. *In* Enzyme Kinetics: Behavior and Analysis of Rapid Equilibrium and Steady-State Enzyme Systems. John Wiley and Sons, New York, NY. 606–626.

Shannon, T. R., and D. M. Bers. 1997. Assessment of intra-SR free [Ca] and buffering in rat heart. *Biophys. J.* 73:1524–1531.

Shannon, T. R., G. Chu, E. Kranias, and D. M. Bers. 2001. Phospholamban decreases the energetic efficiency of the sarcoplasmic reticulum Ca pump. *J. Biol. Chem.* 276:7195–7201.

Shannon, T. R., K. S. Ginsburg, and D. M. Bers. 2000a. Potentiation of fractional SR Ca release by total and free intra-SR Ca concentration. *Biophys. J.* 78:334–343.

Shannon, T. R., K. S. Ginsburg, and D. M. Bers. 2000b. Reverse mode of the SR Ca pump and load-dependent cytosolic Ca decline in voltage clamped cardiac ventricular myocytes. *Biophys. J.* 78:322–333.

Shannon, T. R., K. S. Ginsburg, and D. M. Bers. 2002. Quantitative assessment of the SR Ca^{2+} leak-load relationship. *Circ. Res.* 91:594–600.

Shannon, T. R., T. Guo, and D. M. Bers. 2003a. Ca^{2+} scraps: local depletions of free $[Ca^{2+}]$ in cardiac sarcoplasmic reticulum during contractions leave substantial Ca^{2+} reserve. *Circ. Res.* 93:40–45.

Shannon, T. R., S. M. Pogwizd, and D. M. Bers. 2003b. Elevated sarcoplasmic reticulum Ca leak in intact ventricular myocytes from rabbits in heart failure. *Circulation.* 93:592–594.

Shiferaw, Y., M. A. Watanabe, A. Garfinkel, J. N. Weiss, and A. Karma. 2003. Model of intracellular calcium cycling in ventricular myocytes. *Biophys. J.* 85:3666–3686.

Sipido, K. R., and W. G. Wier. 1991. Flux of Ca^{2+} across the sarcoplasmic reticulum of guinea-pig cardiac cells during excitation-contraction coupling. *J. Physiol.* 435:605–630.

Soeller, C., and M. B. Cannell. 1997. Numerical simulation of local calcium movements during L-type calcium channel gating in the cardiac diad. *Biophys. J.* 73:97–111.

Song, L.-S., M. D. Stern, E. G. Lakatta, and H. Cheng. 1997. Partial depletion of sarcoplasmic reticulum calcium does not prevent calcium sparks in rat ventricular myocytes. *J. Physiol.* 505:665–675.

Spencer, C. I., and J. R. Berlin. 1995. Control of sarcoplasmic reticulum calcium release during calcium loading in isolated rat ventricular myocytes. *J. Physiol.* 488:267–279.

Spencer, C. I., and J. R. Berlin. 1997. Calcium-induced release of strontium ions from the sarcoplasmic reticulum of rat cardiac ventricular myocytes. *J. Physiol.* 504:565–578.

Stern, M. D., L.-S. Song, H. Cheng, J. S. Sham, H. T. Yang, K. R. Boheler, and E. Ríos. 1999. Local control models of cardiac excitation-contraction coupling a possible role for allosteric interactions between ryanodine receptors. *J. Gen. Physiol.* 113:469–489.

Takenaka, H., P. N. Adler, and A. M. Katz. 1982. Calcium fluxes across the membrane of sarcoplasmic reticulum vesicles. *J. Biol. Chem.* 257:12649–12656.

Terentyev, D., S. Viatchenko-Karpinski, H. Valdivia, A. Escobar, and S. Gyorke. 2002. Luminal Ca^{2+} controls termination and refractory behavior of Ca^{2+}-induced Ca^{2+} release in cardiac myocytes. *Circ. Res.* 91:414–420.

Terracciano, C. M. N., R. U. Naqvi, and K. T. MacLeod. 1995. Effects of rest interval on the release of calcium from the sarcoplasmic reticulum in isolated guinea pig ventricular myocytes. *Circ. Res.* 77:354–360.

Tohse, N. 1990. Calcium-sensitive delayed rectifier potassium currents in guinea pig ventricular cells. *Am. J. Physiol.* 258:H1200–H1207.

Trafford, A. W., M. E. Díaz, and D. A. Eisner. 1998. Stimulation of Ca-induced Ca release only transiently increases the systolic Ca transient: measurement of Ca fluxes and sarcoplasmic reticulum Ca. *Cardiovasc. Res.* 37:710–717.

Trafford, A. W., M. E. Diaz, S. C. O'Neill, and D. A. Eisner. 1995. Comparison of subsarcolemmal and bulk calcium concentration during spontaneous calcium release in rat ventricular myocytes. *J. Physiol.* 488:577–586.

Tsien, R. W., P. Hess, E. W. McCleskey, and R. L. Rosenbeg. 1987. Calcium channels: mechanisms of selectivity, permeation and block. *Annu. Rev. Biophys. Chem.* 16:265–290.

Usyk, T. P., and A. D. McCulloch. 2003. Electomechanical model of cardiac resynchronization in the dilated failing heart with left bundle branch block. *J. Electrocardiol.* 36(Suppl.):57–61.

Villalba-Galea, C. A., B. A. Suarez-Isla, M. Fill, and A. L. Escobar. 1998. Kinetic model for ryanodine receptor adaptation. *Biophys. J.* 74:58. (Abstr.)

Weber, C., K. Ginsburg, K. Philipson, T. Shannon, and D. Bers. 2001. Allosteric regulation of Na/Ca exchange current by cytosolic Ca in intact cardiac myocytes. *J. Gen. Physiol.* 117:119–131.

Weber, A., R. Herz, and I. Reis. 1966. Study of the kinetics of calcium transport by isolated fragmented sarcoplasmic reticulum. *Biochem. Z.* 345:329–369.

Weber, C. R., V. Piacentino, K. S. Ginsburg, S. R. Houser, and D. M. Bers. 2002. Na^+-Ca^{2+} exchange current and submembrane $[Ca^{2+}]$ during the cardiac action potential. *Circ. Res.* 90:182–189.

Winslow, R. L., J. Rice, S. Jafri, E. Marban, and B. O'Rourke. 1999. Mechanisms of altered excitation-contraction coupling in canine tachycardia-induced heart failure. II. Model studies. *Circ. Res.* 84:571–586.

Yuan, W., K. S. Ginsburg, and D. M. Bers. 1996. Comparison of sarcolemmal calcium channel current in rabbit and rat ventricular myocytes. *J. Physiol.* 493:733–746.

Zahradnikova, A., and I. Zahradnik. 1996. A minimal gating model for the cardiac calcium release channel. *Biophys. J.* 71:2996–3012.

Zygmunt, A. C., and W. R. Gibbons. 1991. Calcium-activated chloride current in rabbit ventricular myocytes. *Circ. Res.* 68:424–437.